CONTINUUM THEORY OF SELF-SIMILAR DISLOCATION CELLULAR STRUCTURES

A Dissertation

Presented to the Faculty of the Graduate School

of Cornell University

in Partial Fulfillment of the Requirements for the Degree of

Doctor of Philosophy

by

Yong S. Chen

January 2012

© 2012 Yong S. Chen

ALL RIGHTS RESERVED

CONTINUUM THEORY OF SELF-SIMILAR DISLOCATION CELLULAR STRUCTURES

Yong S. Chen, Ph.D.

Cornell University 2012

I present a continuum dislocation dynamics model to explain the emergent mesoscale self-similar cellular dislocation structures observed in plastically-deformed crystals. In three dimensions (3D), we study three distinct physically motivated dynamics which consistently lead to fractal formation with rather similar morphologies, and therefore we suggest that this is a general feature of the 3D collective behavior of dislocations. The striking self-similar features are measured in terms of correlation functions of physical observables, such as the geometrically necessary dislocation (GND) density, the plastic distortion, and the crystalline orientation. Remarkably, all these correlation functions exhibit spatial power-law behaviors, sharing a single underlying universal critical exponent for each type of dynamics.

We use this continuum dislocation dynamics model to study the properties of x-ray diffraction patterns, and explore ways to infer the underlying complex dislocation cellular structures from them. Our emerging dislocation structures display fractal characteristics. We calculate the x-ray diffraction patterns for FCC crystals during uniaxial tensile deformation, and the resulting patterns exhibit *in-situ* intermittent dynamics (peak appearance and disappearance) and transient peak-splitting behavior, similar to recent in-situ x-ray experiments. We provide the corresponding real space information, which shows that these features do not involve subgrain boundary formation in our simulations.

BIOGRAPHICAL SKETCH

The author was born in a beautiful rural town, Wuwei, in the middle of China. When he was five, his father gave him a special birthday gift – "One Hundred Thousand Questions", which was a series of encyclopedia volumes on fundamental laws or principles in all scientific fields, such as math, physics, and chemistry. These books consisted of thousands and thousands of short articles with vivid cartoons, answering all kinds of 'naive' but intriguing questions. He really loved these books, even without fully understanding. Young Yong had a dream – he would be able to answer such unknown questions by himself one day.

Yong did not leave his hometown until he was eighteen. He started his undergraduate at Tsinghua University, one of the best universities in China. From a small rural town to a giant urban city, Yong got closer to his dream.

During the first two years of his college life, Yong immersed himself in libraries and enjoyed learning science such as math, physics and so on. At that time, the Internet was growing at an incredible rate. Yong then got trapped in this fascinating way of living. He gradually forgot his dream. Until the graduation day came, Yong didn't realize that he had been far away from his dream.

It was not too late. Yong continued to study in the accelerator lab of Tsinghua University, as a master graduate student. One year later, he met Wenteng at a ball and fell into love with her. Before they graduated, both of them didn't want to live in the way that they had been familiar with. They wanted to change. In 2005, they got married and flied together to the other side of the earth.

They came to the beautiful rural town of Ithaca. Away from noisy urban life, everything looked very familiar. Yong found the young boy with the dream. He again immersed himself into the beautiful physics world. At the end of his second year of PhD, he started to work with Professor James Sethna. They developed a new continuum

theory of dislocation dynamics and studied complex dislocation cellular morphologies, known as one of the most challenging problems in material science. Yong and his collaborators had enjoyable and effective teamwork. He really loved his work. At the third year of his graduate life, his lovely daughter, Serena, came to the earth in a beautiful spring morning. There were more fun times in his life!

After six years, Yong and his collaborators successfully applied their theory and simulations to unravel the underlying physics behind the emergent fractal dislocation structures. Yong also finished his PhD dissertation defense in September, 2011. It was time for the next destination. Although he loved his research, he still decided to leave academia for a while and try a new life that he had never experienced. Now Yong and his family will start a new journey in California.

To my lovely wife Wenteng and little princess Serena.

ACKNOWLEDGEMENTS

It is exceedingly memorable that I have spent six years living and studying in this beautiful town of Ithaca. With great pleasure, I would like to express my heartfelt appreciation to many people who have helped me throughout my academic career.

First, I am deeply grateful to my graduate advisor James Sethna. His great enthusiasm and optimism for science infects me; his remarkable intuition about physics amazes me; his insightful guidance motivates me. He always makes me excited for my work. I really feel that I have been so lucky to work with him. I also thank the other members of my special committee, Veit Elser and Itai Cohen. Their intriguing comments and suggestions make my work more exciting.

I would like to acknowledge the contribution of my colleagues and coauthors – Woosong Choi, Stefanos Papanikolaou, and Matthew Bierbaum. We had enjoyable teamwork and good times during the past few years. They explored sophisticated numerical algorithm for solving shock wave dynamics, utilized fascinating GPU techniques to set up large-scale simulations, and provided helpful insights on data analysis. I also thank other members of the Sethna group for their help. I have been remembering all fun times in our group. I would like to thank everyone in the fifth floor of Clark Hall, especially Douglas Milton, Connie Wright, and Judy Wilson for helping me deal with all kinds of things, from borrowing keys to filling out travel reimbursement form.

I am very grateful to my mechanical engineering colleagues at Cornell, including Matthew Miller, Paul Dawson and Derek Warner. We have spent great time reading research papers and sharing insightful ideas. After every brainstorming meeting, I have been always inspired by their valuable inputs. I would like to thank my mathematical colleague Alexander Vladimirsky for explaining the frontier of solving singular partial differential equations. I also thank my physical colleague Eric Siggia for his helpful discussions on the turbulent dislocation flow.

During six years of my graduate career, I have been funded by the Basic Energy Sciences (BES) program of Department of Energy (DOE) through DE-FG02-07ER46393, for three semesters. My work has been partially supported by the National Center for Supercomputing Applications under MSS090037 and utilized the Lincoln and Abe clusters.

Last but most importantly, I would like to thank my family, particularly my wife Wenteng and my daughter Serena, for their endless love and support.

TABLE OF CONTENTS

Biographical Sketch . . . iii
Dedication . . . v
Acknowledgements . . . vi
Table of Contents . . . viii
List of Tables . . . x
List of Figures . . . xi

1 Overview **1**

2 Continuum dislocation dynamics (CDD) **5**
2.1 Introduction . . . 5
2.2 Order parameter fields . . . 6
2.2.1 Conserved order parameter field . . . 6
2.2.2 Non-conserved order parameter field . . . 10
2.3 Free energy functional . . . 11
2.4 Traditional dissipative continuum dynamics . . . 12
2.4.1 Dissipative dynamics built from the non-conserved order parameter field β^{p} . . . 12
2.4.2 Dissipative dynamics built from the conserved order parameter field ϱ . . . 13
2.5 Our CDD model . . . 16
2.5.1 Climb and glide dynamics (CGD) . . . 18
2.5.2 Glide-only dynamics: mobile dislocation population (GOD-MDP) 19
2.5.3 Glide-only dynamics: local vacancy-induced pressure (GOD-LVP) . . . 20
2.6 Coupling to vacancies . . . 22
2.7 Incorporating slip systems . . . 23
2.8 Coupling to disorder . . . 27

3 Simulations **29**
3.1 Introduction . . . 29
3.2 Methods . . . 29
3.3 Gaussian random initial conditions . . . 30
3.4 Two dimensional simulations . . . 33
3.5 Three dimensional simulations . . . 37

4 Morphological analysis **41**
4.1 Introduction . . . 41
4.2 Cell boundary characterization . . . 43
4.2.1 Our boundary-pruning method . . . 43
4.3 Fractal analysis . . . 44
4.3.1 Box counting method . . . 44

4.4 Single length scale analysis 46
4.4.1 Distributions of cell sizes and misorientation angles 46
4.4.2 Statistical analysis of misorientation angle distribution 48
4.4.3 Power laws of cell sizes and misorientation angles 48
4.5 Real space renormalization group analysis 49

5 Correlation functions 51
5.1 Introduction 51
5.2 Correlation functions of physical observables 51
5.2.1 Correlation function of crystalline orientation field 52
5.2.2 Correlation function of GND density field 54
5.2.3 Correlation function of plastic distortion field 54
5.3 Correlation functions of the strain-history-dependent plastic deformation and distortion fields 58
5.4 Other correlation functions 63
5.4.1 Stress-stress correlation functions 63
5.4.2 Energy density spectrum 64
5.4.3 Correlation function of the stressful part of GND density 66
5.5 Finite size effects 67

6 Scaling theory 72
6.1 Introduction 72
6.2 Analytical relations between correlation functions of physical observables 72
6.2.1 C^{ρ} and $C^{\mathbf{\Lambda}}$ 73
6.2.2 $C^{\beta^{\mathrm{p,I}}}$ and $C^{\mathbf{\Lambda}}$ 74
6.3 Single underlying critical exponent for physical observables 77
6.4 Scaling relations between stress-related correlation functions 80

7 X-ray diffraction 81
7.1 Introduction 81
7.2 Simulations 84
7.3 Incoherent X-ray diffraction: evolution of subgrain structures 85

8 Conclusion 91

A Physical quantities in terms of the plastic distortion tensor 93

B Calculation of energy functional derivative with respect to the GND density 94

C Energy dissipation rate 95

D Summary of dynamical equations of our CDD model 97

LIST OF TABLES

5.1 Critical exponents for correlation functions of strain-history-dependent fields at stress-free states 63

6.1 Critical exponents for correlation functions at stress-free states 79

6.2 Power-laws relations among $\widetilde{C}^{\sigma}(k)$, $E(k)$, and $\widetilde{C}^{\rho^E}(k)$ 80

LIST OF FIGURES

1.1 Mesoscopic coarse-grained model bridges atoms and aircraft 2

2.1 Representation of the crystalline line defect—dislocation 7
2.2 Relaxation of various CDD models 17

3.1 Gaussian random initial conditions with the correlated length scale $0.28L$ in two dimensions 32
3.2 Complex dislocation structures in two dimensions (1024^2) for the relaxed states of an initially random distortion 34
3.3 The elastic free energy decreases to zero as a power law in time in two dimensions 35
3.4 Complex dislocation structures under anisotropic loadings in two dimensions (1024^2) 36
3.5 The elastic free energy decreases to zero as a power law in time in three dimensions 37
3.6 Complex dislocation structures in three dimensions (128^3) for the relaxed states of an initially random distortion 38
3.7 Complex dislocation structures under anisotropic loadings in three dimensions (128^3) 39

4.1 Theoretical and experimental dislocation fractal morphologies 42
4.2 Cellular structures under strain 43
4.3 Box-counting fractal dimension before & during external strain 45
4.4 Dependence of the fractal dimensions on minimum square misorientation threshold θ_c^2 45
4.5 Cellular structures under strain: cell size distributions 46
4.6 Cellular structures under strain: misorientation angle distributions . . . 47
4.7 Average misorientation angles versus strain 48
4.8 Average misorientation angles versus strain 49
4.9 Self-similarity in real space 50

5.1 Correlation functions of $\mathbf{\Lambda}$ in both two and three dimensions 53
5.2 Correlation functions of ϱ in both two and three dimensions 55
5.3 Correlation functions of β^{p} in two dimensions 56
5.4 Correlation functions of $\beta^{\mathrm{p,I}}$ in both two and three dimensions 57
5.5 Strain-history-dependent fields $\beta^{\mathrm{p,H}}$ and $\boldsymbol{\psi}$ in two dimensions 59
5.6 Correlation functions of $\beta^{\mathrm{p,H}}$ in both two and three dimensions 60
5.7 Correlation functions of $\boldsymbol{\psi}$ in both two and three dimensions 62
5.8 Stress-stress correlation functions $\widetilde{C}^{\sigma}(k)$, elastic energy spectrum $E(k)$, correlation functions of the stressful part of GND density $\widetilde{C}^{\rho^E}(k)$ 65
5.9 Relaxation with various initial length scales in two dimensions 68
5.10 Statistical convergence of correlation functions of Λ, ρ and $\beta^{\mathrm{p,I}}$ by varying lattice sizes in two dimensions 70

5.11 Statistical convergence of correlation functions of Λ, ρ and $\beta^{\mathrm{p,I}}$ by varying the initial length scales in 1024^2 simulations 71

7.1 Complex dislocation structures under uniaxial tensile deformation in two dimensions (1024^2) 84
7.2 Schematic plot of the X-ray diffraction simulation 85
7.3 Full diffraction pattern 87
7.4 Subgrain dynamics: peak appearance and disappearance 88
7.5 Subgrain dynamics: peak division and recombination 89

CHAPTER 1

OVERVIEW

Blacksmiths make horseshoes by heating, beating and bending iron. It has been a long mystery what happens to the metal's individual atoms during such a process. Since late in the last century, the complex interaction among crystal dislocations have been recognized for dominating macroscopic characteristics, such as morphological, mechanical, and thermodynamic properties, of engineering materials.

Dislocations are line defects in structural materials. At the microscopic scale, atomistic models or discrete dislocation dynamics are sufficient to describe the motion of individual or small numbers of dislocations. At the macroscopic scale, characteristic properties of engineering materials are extensively studied by continuum mechanics or finite element analysis. Figure 1 shows a huge gap between them, which demands an appropriate mesoscopic model to connect them.

In plastically deformed engineering materials, an enormous number of dislocations move in a collective fashion. They self-interact, annihilate, and tangle together. Meanwhile, they also interact with point defects and all kinds of impurities. From the engineering point of view, a good model should take into account all possible factors that affect the motion of dislocations. However, from our physics point of view, we would like to start from a minimal model which captures the underlying physics of collective dislocation motions, and then take into account other possible mechanisms that change the collective behavior of dislocations.

This thesis is organized into eight chapters. In this chapter, we give a general overview to physical modeling at various length scales varying from nanometer to meter, and address the importance of mesoscopic coarse-grained models, which is the focus of

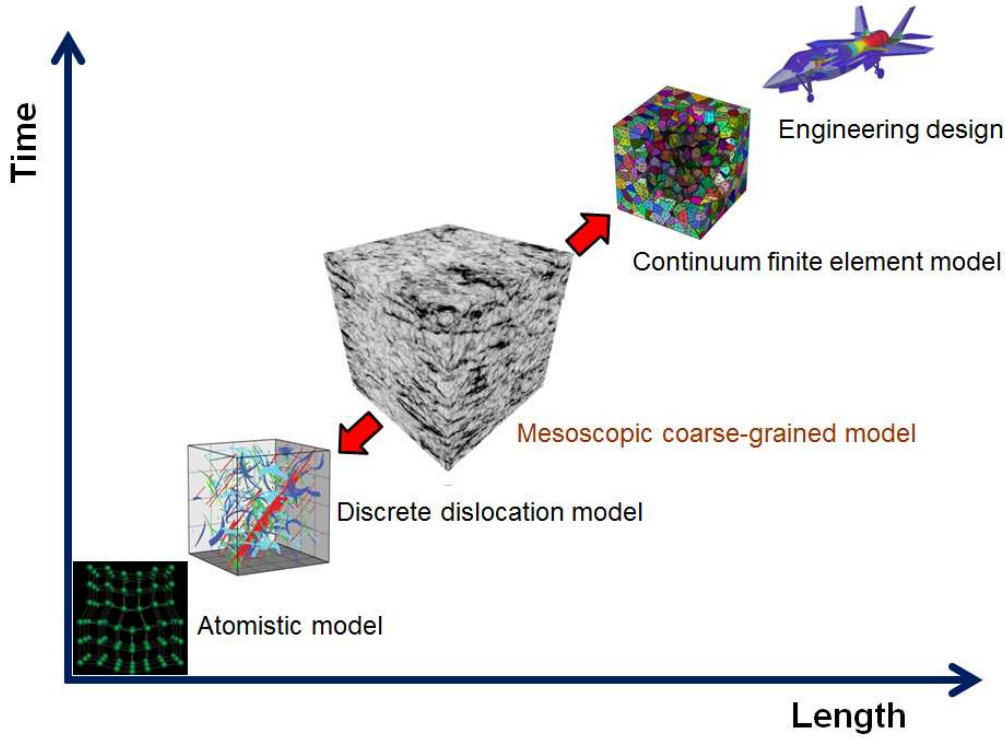

Figure 1.1: **Mesoscopic coarse-grained model bridges atoms and aircraft.** The mesoscopic model, built from the microscopic physics, provides essential inputs to the macroscopic modeling.

this thesis.

In chapter 2, we introduce the order parameters generally used in continuum plasticity theories, and derive standard local dynamical evolution laws using traditional condensed matter approaches, starting from both the conserved and non-conserved order parameter fields. We explain why these resulting dynamical laws are not appropriate at the mesoscale. we show how to extend this approach by defining appropriate constitutive laws for the dislocation flow velocity to build novel dynamics [1]. There are three different dynamics we study: i) isotropic climb-and-glide dynamics (CGD) [2–6], ii) isotropic glide-only dynamics, where we define the part of the local dislocation density that participates in the local *mobile dislocation population*, keeping the local volume conserved at all times (GOD-MDP) [7], iii) isotropic glide-only dynamics, where glide

is enforced by a *local vacancy pressure* due to a co-existing background of vacancies that have an infinite energy cost (GOD-LVP) [8]. All three types of dynamics present physically valid alternative approaches for deriving a coarse-grained continuum model for GNDs.

In chapter 3, We briefly introduce the numerical methods used in our simulations, which are appropriate for solving shock-forming partial differential equations. We introduce the non-trivial random initial conditions and discuss the resulting simulations of both two and three dimensional relaxation and loading.

In chapter 4, we introduce our boundary pruning method to cluster the cellular structures into characteristic cells. Then we perform experimental morphological analysis. We can apply the box counting method on the resulting cell boundaries to characterize the fractal dimension. Also, we can collect the statistical information of cell sizes and misorientation angles, and analyze their scaling functions.

In fact, the emergent self-similar structures can be well described by a generic scaling theory. In chapter 5, we measure correlation functions of physical observables, such as the plastic distortion, the geometrically necessary dislocation, and the crystalline orientation. They all exhibit power-law behaviors. We also measure the correlation functions of the strain-history-dependent plastic deformation and distortion fields, and the stress-related correlation functions.

In chapter 6, we analytically find out the relations among correlation functions of these physical observables, and show that they are all described by a single underlying critical exponent by applying ideas from the renormalization group.

In chapter 7, we simulate the x-ray diffraction patterns for FCC crystals during uniaxial tensile deformation. The resulting patterns exhibit *in-situ* intermittent dynamics

(peak appearance and disappearance) and transient peak-splitting behavior, similar to recent in-situ x-ray experiments. We provide the corresponding real space information, showing that these features do not involve subgrain boundary formation in our simulations. We summarize our work in chapter 8.

In this thesis, we provide a flexible framework of CDD to study mesoscale phenomena due to the collective motion of dislocations. The key feature of our resulting simulation patterns is the emergent self-similarity, which has been characterized by a single underlying critical exponent shared by the correlation functions of the GND density, the crystalline orientation, and the intrinsic part of the plastic distortion. Our CDD model provides a new example of self-organized critical dynamics and pattern formation.

CHAPTER 2

CONTINUUM DISLOCATION DYNAMICS (CDD)[1]

2.1 Introduction

Dislocations in plastically deformed crystals, driven by their long-range interactions, collectively evolve into complex heterogeneous structures where dislocation-rich cell walls or boundaries surround dislocation-depleted cell interiors. These have been observed both in single crystals [9–11] and polycrystals [12] using transmission electron microscopy (TEM). The mesoscopic cellular structures have been recognized as scale-free patterns through fractal analyses of TEM micrographs [13–16]. The complex collective behavior of dislocations has been a challenge for understanding the underlying physical mechanisms responsible for the development of emergent dislocation morphologies.

Complex dislocation microstructures, as an emergent mesoscale phenomenon, have been previously modeled using various theoretical and numerical approaches. Discrete dislocation dynamics (DDD) models have provided insights into the dislocation pattern formations: parallel edge dislocations in a two-dimensional system evolve into 'matrix structures' during single slip [17], and 'fractal and cell structures' during multiple slip [18, 19]; random dislocations in a three-dimensional system self-organize themselves into microstructures through junction formation, cross-slip, and short-range interactions [20, 21]. However, DDD simulations are limited by the computational challenges on the relevant scales of length and strain. Beyond these micro-scale descriptions, continuum dislocation dynamics (CDD) has also been used to study complex

[1]This chapter is part of a preprint (arXiv:1106.0195) in collaboration with Woosong Choi, Stefanos Papanikolaou, Matthew Bierbaum, and James Sethna. This manuscript has been submitted to Physical Review B.

dislocation structures. Simplified reaction-diffusion models have described persistent slip bands [22], dislocation cellular structures during multiple slip [23], and dislocation vein structures [24]. Stochasticity in CDD models [15, 17, 25] or in the splittings and rotations of the macroscopic cells [26–28] have been suggested as an explanation for the formation of organized dislocation structures. The source of the noise in these stochastic theories is derived from either extrinsic disorder or short length-scale fluctuations.

Recently, our CDD model has been developed [5–7] which predicts the formation of dislocation cellular microstructures, exhibiting an emergent self-similarity [7]. In this chapter, we present the CDD model in detail.

2.2 Order parameter fields

2.2.1 Conserved order parameter field

A dislocation is the topological defect of a crystal lattice. In a continuum theory, it can be described by a coarse-grained variable, the GND density [2], (also called the net dislocation density or the Nye dislocation density), which can be defined by the GND density tensor

$$\rho(\mathbf{x}) = \sum_{\alpha} (\hat{\mathbf{t}}^{\alpha} \cdot \hat{\mathbf{n}}) \hat{\mathbf{n}} \otimes \mathbf{b}^{\alpha} \delta(\mathbf{x} - \boldsymbol{\xi}^{\alpha}), \tag{2.1}$$

so

$$\rho_{km}(\mathbf{x}) = \sum_{\alpha} \hat{t}_k^{\alpha} b_m^{\alpha} \delta(\mathbf{x} - \boldsymbol{\xi}^{\alpha}), \tag{2.2}$$

[2]Dislocations which cancel at the macroscale may be geometrically necessary at the mesoscale. The distinction between GND and SSD (statistically stored dislocations, also called geometrically unnecessary dislocations) depends on the coarse-graining length scale. At the mesoscopic scale of dislocation pattern formation, GNDs dominate the dynamics.

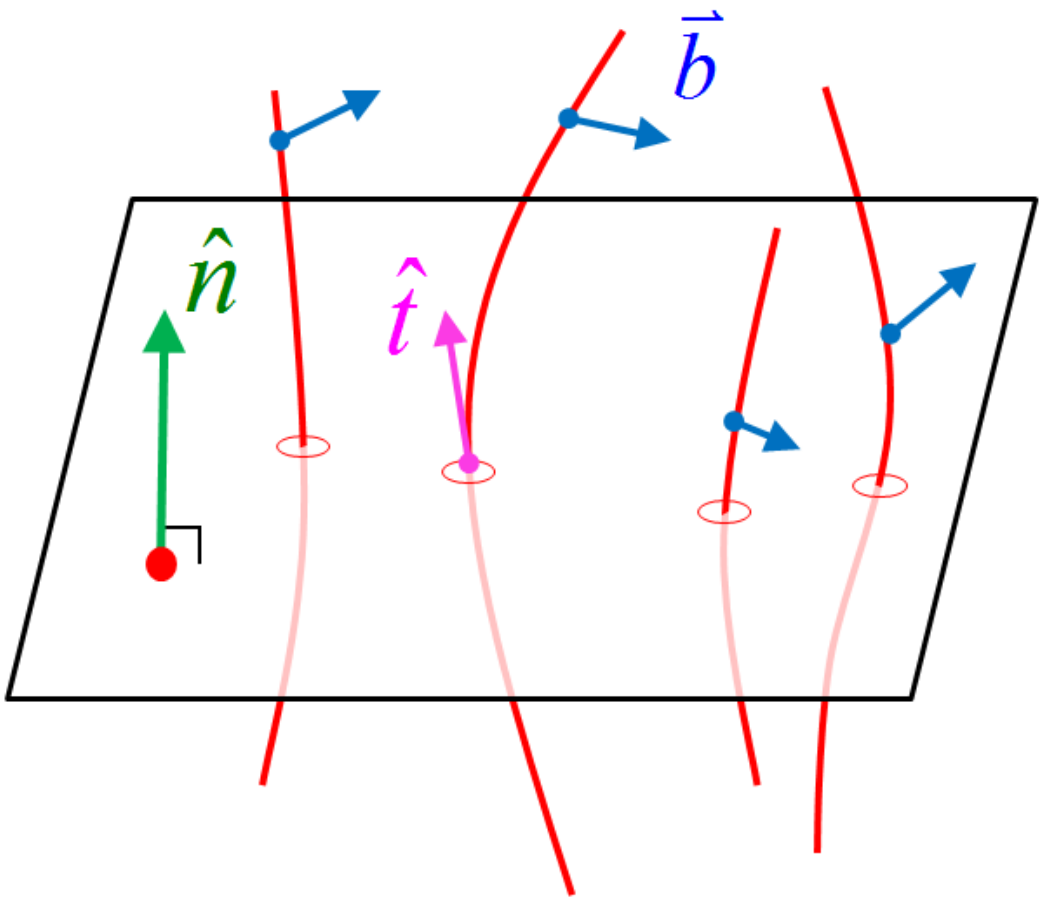

Figure 2.1: **Representation of the crystalline line defect—dislocation.** Each curved line represents a dislocation line with the tangent direction $\hat{\mathbf{t}}$, and the Burgers vector $\mathbf{b}$ which characterizes the magnitude and direction of the distortion to the lattice. The two-index GND density ρ_{km} (Eqs. 2.1 and 2.2) is the net flux of the Burgers vector density $\mathbf{b}$ along $\hat{\mathbf{e}}^{(m)}$ through an infinitesimal piece of a plane with normal direction $\hat{\mathbf{n}}$ along $\hat{\mathbf{e}}^{(k)}$. The three-index version ϱ_{ijm} (Eqs. 2.3 and 2.4) is the flux density through the plane along the axes $\hat{\mathbf{e}}^{(i)}$ and $\hat{\mathbf{e}}^{(j)}$, with the unit bivector $\hat{E} = \hat{\mathbf{e}}^{(i)} \wedge \hat{\mathbf{e}}^{(j)}$.

measuring the sum of the net flux of dislocations α located at ξ, tangent to $\hat{\mathbf{t}}$, with Burgers vector $\mathbf{b}$, in the neighborhood of $\mathbf{x}$, through an infinitesimal plane with the normal direction along $\hat{\mathbf{n}}$, seen in Fig. 2.1. In the continuum, the discrete sum of line singularities in Eqs. (2.1) and (2.2) is smeared into a continuous (nine-component) field, just as the continuum density of a liquid is at root a sum of point contributions from atomic nuclei.

Since the normal unit pseudovector $\hat{\mathbf{n}}$ is equivalent to an antisymmetric unit bivector $\hat{E}$, $\hat{E}_{ij} = \varepsilon_{ijk}\hat{n}_k$, we can reformulate the GND density as a three-index tensor

$$\varrho(\mathbf{x}) = \sum_{\alpha} (\hat{\mathbf{t}}^{\alpha} \cdot \hat{\mathbf{n}}) \hat{E} \otimes \mathbf{b}^{\alpha} \delta(\mathbf{x} - \boldsymbol{\xi}^{\alpha}), \tag{2.3}$$

so

$$\varrho_{ijm}(\mathbf{x}) = \sum_{\alpha} (\hat{\mathbf{t}}^{\alpha} \cdot \hat{\mathbf{n}}) \hat{E}_{ij} b^{\alpha}_{m} \delta(\mathbf{x} - \boldsymbol{\xi}^{\alpha}), \tag{2.4}$$

measuring the same sum of the net flux of dislocations in the neighborhood of $\mathbf{x}$, through the infinitesimal plane indicated by the unit bivector $\hat{E}$. This three-index variant will be useful in Sec. 2.5.2, where we adapt the equations of Refs. [5] and [6] to forbid dislocation climb.

According to the definition of $\hat{E}$, we can find the relation between ρ and ϱ

$$\varrho_{ijm}(\mathbf{x}) = \sum_{\alpha} (\hat{t}^{\alpha}_{l} \hat{n}_l) \varepsilon_{ijk} \hat{n}_k b^{\alpha}_{m} \delta(\mathbf{x} - \boldsymbol{\xi}^{\alpha}) = \varepsilon_{ijk} \rho_{km}(\mathbf{x}). \tag{2.5}$$

It should be noted here that dislocations cannot terminate within the crystal, implying that

$$\partial_i \rho_{ij}(\mathbf{x}) = 0, \tag{2.6}$$

or

$$\varepsilon_{ijk} \partial_k \varrho_{ijl}(\mathbf{x}) = 0. \tag{2.7}$$

Within plastic theories, the gradient of the total displacement field $\mathbf{u}$ represents the compatible total distortion field [29] $\beta_{ij} = \partial_i u_j$, which is the sum of the elastic and the plastic distortion fields [29], $\beta = \beta^{\mathrm{p}} + \beta^{\mathrm{e}}$. Due to the presence of dislocation lines, both β^{p} and β^{e} are incompatible, characterized by the GND density ρ

$$\rho_{ij} = \epsilon_{ilm} \partial_l \beta^{\mathrm{e}}_{mj}, \tag{2.8}$$

$$= -\epsilon_{ilm} \partial_l \beta^{\mathrm{p}}_{mj}. \tag{2.9}$$

The elastic distortion field β^{e} is the sum of its symmetric strain and antisymmetric rotation fields,

$$\beta^{\mathrm{e}} = \epsilon^{\mathrm{e}} + \omega^{\mathrm{e}}, \tag{2.10}$$

where we assume linear elasticity, ignoring the 'geometric nonlinearity' in these tensors. Substituting the sum of two tensor fields into the incompatibility relation Eq. (2.8) gives

$$\rho_{ij} = \varepsilon_{ikl}\partial_k\omega^{\mathrm{e}}_{lj} + \varepsilon_{ikl}\partial_k\epsilon^{\mathrm{e}}_{lj}. \tag{2.11}$$

The elastic rotation tensor ω^{e} can be rewritten as an axial vector, the crystalline orientation vector $\mathbf{\Lambda}$

$$\Lambda_k = \frac{1}{2}\varepsilon_{ijk}\omega^{\mathrm{e}}_{ij}, \tag{2.12}$$

or

$$\omega^{\mathrm{e}}_{ij} = \varepsilon_{ijk}\Lambda_k. \tag{2.13}$$

Thus we can substitute Eq. (2.13) into Eq. (2.11)

$$\rho_{ij} = (\delta_{ij}\partial_k\Lambda_k - \partial_j\Lambda_i) + \varepsilon_{ikl}\partial_k\epsilon^{\mathrm{e}}_{lj}. \tag{2.14}$$

For a system without residual elastic stress, the GND density thus depends only on the varying crystalline orientation [30].

Dynamically, the time evolution law of the GND density emerges from the conservation of the Burgers vector

$$\frac{\partial}{\partial t}\rho_{ik} = -\varepsilon_{ijq}\partial_j J_{qk}, \tag{2.15}$$

or

$$\frac{\partial}{\partial t}\varrho_{ijk} = -\varepsilon_{ijm}\varepsilon_{mpq}\partial_p J_{qk} = -g_{ijpq}\partial_p J_{qk}, \tag{2.16}$$

where J represents the Burgers vector flux, and the symbol g_{ijpq} indicates $\varepsilon_{ijm}\varepsilon_{mpq} = \delta_{ip}\delta_{jq} - \delta_{iq}\delta_{jp}$.

2.2.2 Non-conserved order parameter field

The natural physicist's order parameter field ϱ, characterizing the incompatibility, can be written in terms of the plastic distortion field β^{p}

$$\varrho_{ijk} = \varepsilon_{ijm}\rho_{mk} = -g_{ijls}\partial_l\beta^{\mathrm{p}}_{sk}. \tag{2.17}$$

In the linear approximation, the alternative order parameter field β^{p} fully specifies the local deformation $\boldsymbol{u}$ of the material, the elastic distortion β^{e}, the internal long-range stress field σ^{int} and the crystalline orientation (the Rodrigues vector $\boldsymbol{\Lambda}$ giving the axis and angle of rotation), as summarized in Appendix A.

According to Eq. (2.9) and Eq. (2.15), the flux J of the Burgers vector can be expressed in terms of the dynamics of the plastic distortion tensor β^{p}

$$\frac{\partial\beta^{\mathrm{p}}_{ij}}{\partial t} = J_{ij}. \tag{2.18}$$

The plastic distortion β^{p} can be specified by the GND density ρ and a strain-history deformation field $\boldsymbol{\psi}$ in Fourier space [3],

$$\begin{aligned}\widetilde{\beta}^{\mathrm{p}}_{ij}(\mathbf{k}) &= -i\varepsilon_{ilm}\frac{k_l}{k^2}\widetilde{\rho}_{mj}(\mathbf{k}) + ik_i\widetilde{\psi}_j(\mathbf{k}) \\ &\equiv \widetilde{\beta}^{\mathrm{p,I}}_{ij}(\mathbf{k}) + \widetilde{\beta}^{\mathrm{p,H}}_{ij}(\mathbf{k}),\end{aligned} \tag{2.19}$$

hence decomposing $\widetilde{\beta}^{\mathrm{p}}$ into two parts. $\beta^{\mathrm{p,I}}$ is the intrinsic field specified by the GND density. Similar to ρ, $\beta^{\mathrm{p,I}}$ is also divergence free: $\partial_i\beta^{\mathrm{p,I}}_{ij} = 0$, i.e., $k_i\widetilde{\beta}^{\mathrm{p,I}}_{ij} = 0$. $\beta^{\mathrm{p,H}}$ is a (curl-free) gradient of $\boldsymbol{\psi}$, depending upon the strain history and contributing nothing to the GND density. This decomposition will become important to us in Sec. 5.2, where the correlation functions of $\beta^{\mathrm{p,I}}$ and $\beta^{\mathrm{p,H}}$ will scale differently with distance.

[3] In Fourier space, the zero mode of β^{p} can not be obtained from the GND density field. In the context of the correlation function of β^{p}, the zero mode is eliminated because we subtract fields at different sites before correlating.

2.3 Free energy functional

In the absence of external stress, the free energy $\mathcal{F}$ is the elastic energy caused by the internal long-range stress

$$\mathcal{F} = \int d^3\mathbf{x}\ \frac{1}{2}\sigma^{\text{int}}_{ij}\epsilon^{\text{e}}_{ij} = \int d^3\mathbf{x}\ \frac{1}{2}C_{ijmn}\epsilon^{\text{e}}_{ij}\epsilon^{\text{e}}_{mn}, \tag{2.20}$$

where the stress is $\sigma^{\text{int}}_{ij} = C_{ijmn}\epsilon^{\text{e}}_{mn}$, with C_{ijmn} the stiffness tensor.

Using the symmetry of C_{ijmn} and ignoring large rotations, $\epsilon^{\text{e}}_{ij} = (\beta^{\text{e}}_{ij} + \beta^{\text{e}}_{ji})/2$, we can rewrite the elastic energy $\mathcal{F}$ in terms of β^{e}

$$\mathcal{F} = \int d^3\mathbf{x}\ \frac{1}{2}C_{ijmn}\beta^{\text{e}}_{ij}\beta^{\text{e}}_{mn}. \tag{2.21}$$

Performing a Fourier transform on both β^{p}_{ij} and β^{p}_{mn} simultaneously gives

$$\mathcal{F} = \int d^3\mathbf{x} \int \frac{d^3\mathbf{k}}{(2\pi)^3} \int \frac{d^3\mathbf{k}'}{(2\pi)^3}\ e^{i(\mathbf{k}+\mathbf{k}')\mathbf{x}}\left(\frac{1}{2}C_{ijmn}\widetilde{\beta}^{\text{e}}_{ij}(\mathbf{k})\widetilde{\beta}^{\text{e}}_{mn}(\mathbf{k}')\right). \tag{2.22}$$

Integrating out the spatial variable $\mathbf{x}$ leaves a $\delta-$function $\delta(\mathbf{k} + \mathbf{k}')$ in Eq. (2.22). We hence integrate out the k-space variable $\mathbf{k}'$

$$\mathcal{F} = \int \frac{d^3\mathbf{k}}{(2\pi)^3}\ \frac{1}{2}C_{ijmn}\widetilde{\beta}^{\text{e}}_{ij}(\mathbf{k})\widetilde{\beta}^{\text{e}}_{mn}(-\mathbf{k}). \tag{2.23}$$

Substituting Eq. (A.2) into Eq. (2.23) gives

$$\begin{aligned}\mathcal{F} &= \int \frac{d^3\mathbf{k}}{(2\pi)^3}\ \frac{1}{2}(C_{ijmn}T_{ijpq}(\mathbf{k})T_{mnst}(-\mathbf{k}))\widetilde{\beta}^{\text{p}}_{pq}(\mathbf{k})\widetilde{\beta}^{\text{p}}_{st}(-\mathbf{k}) \\ &= -\int \frac{d^3\mathbf{k}}{(2\pi)^3}\ \frac{1}{2}M_{pqst}(\mathbf{k})\widetilde{\beta}^{\text{p}}_{pq}(\mathbf{k})\widetilde{\beta}^{\text{p}}_{st}(-\mathbf{k}),\end{aligned} \tag{2.24}$$

where we skip straightforward but tedious simplifications.

In the presence of external loading, we can express the appropriate free energy $\mathcal{F}$ as the sum of two terms: the elastic interaction energy of GNDs, and the energy of

interaction with the applied stress field. The free energy functional is

$$\mathcal{F} = \int d^3\mathbf{x}\Big(\frac{1}{2}\sigma^{\text{int}}_{ij}\epsilon^{\text{e}}_{ij} - \sigma^{\text{ext}}_{ij}\epsilon^{\text{p}}_{ij}\Big). \tag{2.25}$$

Alternatively, it can be rewritten in Fourier space

$$\mathcal{F} = -\int \frac{d^3\mathbf{k}}{(2\pi)^3}\Big(\frac{1}{2}M_{ijmn}(\mathbf{k})\widetilde{\beta}^{\text{p}}_{ij}(\mathbf{k})\widetilde{\beta}^{\text{p}}_{mn}(-\mathbf{k}) + \widetilde{\sigma}^{\text{ext}}_{ij}(\mathbf{k})\widetilde{\beta}^{\text{p}}_{ij}(-\mathbf{k})\Big). \tag{2.26}$$

2.4 Traditional dissipative continuum dynamics

There are well known approaches for deriving continuum equations of motion for dissipative systems, which in this case produce a traditional von Mises-style theory [31] at the mesoscale, useful at longer scales. We begin by reproducing these standard equations.

For the sake of simplicity, we ignore external stress (σ_{ij} simplified to σ^{int}_{ij}) in the following three subsections. We start by using the standard methods applied to the non-conserved order parameter β^{p}, and then turn to the conserved order parameter ϱ.

2.4.1 Dissipative dynamics built from the non-conserved order parameter field β^{p}

The plastic distortion β^{p} is a non-conserved order parameter field, which is utilized by the engineering community to study texture evolutions and plasticity of mechanically deformed structural materials. The simplest dissipative dynamics in terms of β^{p} minimizes the free energy by steepest decents

$$\frac{\partial}{\partial t}\beta^{\text{p}}_{ij} = -\Gamma\frac{\delta\mathcal{F}}{\delta\beta^{\text{p}}_{ij}}, \tag{2.27}$$

where Γ is a positive material-dependent constant. We may rewrite it in Fourier space, giving

$$\frac{\partial}{\partial t}\widetilde{\beta}^{\mathrm{p}}_{ij}(\mathbf{k}) = -\Gamma\frac{\delta\mathcal{F}}{\delta\widetilde{\beta}^{\mathrm{p}}_{ij}(-\mathbf{k})}. \tag{2.28}$$

The functional derivative $\delta\mathcal{F}/\delta\widetilde{\beta}^{\mathrm{p}}_{ij}(-\mathbf{k})$ is the negative of the long-range stress

$$\frac{\delta\mathcal{F}}{\delta\widetilde{\beta}^{\mathrm{p}}_{ij}(-\mathbf{k})} = -M_{ijmn}(\mathbf{k})\widetilde{\beta}^{\mathrm{p}}_{mn}(\mathbf{k}) \equiv -\widetilde{\sigma}_{ij}(\mathbf{k}). \tag{2.29}$$

This dynamics implies a simplified version of von Mises plasticity

$$\frac{\partial}{\partial t}\widetilde{\beta}^{\mathrm{p}}_{ij}(\mathbf{k}) = \Gamma\widetilde{\sigma}_{ij}(\mathbf{k}). \tag{2.30}$$

2.4.2 Dissipative dynamics built from the conserved order parameter field ϱ

We can also derive an equation of motion starting from the GND density ϱ, as was done by Rickman and Viñals [31]. For this dissipative dynamics Eq. (2.16), the simplest expression for J is

$$J_{qk} = -\Gamma'_{ablq}\partial_l\frac{\delta\mathcal{F}}{\delta\varrho_{abk}}, \tag{2.31}$$

where the material-dependent constant tensor Γ' must be chosen to guarantee a decrease of the free energy with time.

The infinitesimal change of $\mathcal{F}$ with respect to the GND density ϱ is

$$\delta\mathcal{F}[\varrho] = \int d^3\mathbf{x}\ \frac{\delta\mathcal{F}}{\delta\varrho_{ijk}}\delta\varrho_{ijk}. \tag{2.32}$$

The free energy dissipation rate is thus $\delta\mathcal{F}/\delta t$ for $\delta\varrho = \frac{\partial\varrho}{\partial t}\delta t$, hence

$$\frac{\partial}{\partial t}\mathcal{F}[\varrho] = \int d^3\mathbf{x}\ \frac{\delta\mathcal{F}}{\delta\varrho_{ijk}}\frac{\partial\varrho_{ijk}}{\partial t}. \tag{2.33}$$

Substituting Eq. (2.16) into Eq. (2.33) and integrating by parts gives

$$\frac{\partial}{\partial t}\mathcal{F}[\varrho] = \int d^3\mathbf{x}\left(g_{ijpq}\partial_p\frac{\delta\mathcal{F}}{\delta\varrho_{ijk}}\right)J_{qk}. \tag{2.34}$$

Substituting Eq. (2.31) into Eq. (2.34) gives

$$\frac{\partial}{\partial t}\mathcal{F}[\varrho] = -\int d^3\mathbf{x}\left(g_{ijpq}\partial_p\frac{\delta\mathcal{F}}{\delta\varrho_{ijk}}\right)\left(\Gamma'_{ablq}\partial_l\frac{\delta\mathcal{F}}{\delta\varrho_{abk}}\right). \tag{2.35}$$

Now, to guarantee that energy never increases, we choose $\Gamma'_{ablq} = \Gamma g_{ablq}$, ($\Gamma$ is a positive material-dependent constant), which yields the rate of change of energy as a negative of a perfect square

$$\frac{\partial}{\partial t}\mathcal{F}[\varrho] = -\int d^3\mathbf{x}\,\Gamma\sum_{q,k}\left(g_{ablq}\partial_l\frac{\delta\mathcal{F}}{\delta\varrho_{abk}}\right)^2. \tag{2.36}$$

Using Eqs. (2.16) and (2.31), we can write the dynamics in terms of ϱ

$$\frac{\partial}{\partial t}\varrho_{ijk} = \Gamma g_{ijpq}g_{ablq}\partial_p\partial_l\frac{\delta\mathcal{F}}{\delta\varrho_{abk}}. \tag{2.37}$$

Substituting the functional derivative $\delta\mathcal{F}/\delta\varrho_{abk}$, Eq. (B.4), derived in Appendix B, into Eq. (2.37) and comparing to Eq. (2.16) tells us

$$\frac{\partial}{\partial t}\varrho_{ijk}(\mathbf{x}) = -\Gamma g_{ijpq}\partial_p\sigma_{qk}(\mathbf{x}) = -g_{ijpq}\partial_p J_{qk}(\mathbf{x}), \tag{2.38}$$

where

$$J_{qk} = \Gamma\sigma_{qk} \tag{2.39}$$

duplicating the von Mises law (Eq. (2.30)) of the previous subsection.

The simplest dissipative dynamics of either non-conserved or conserved order parameter fields thus turns out to be the traditional linear dynamics, a simplified von Mises law.

The problem with this law for us is that it allows for plastic deformation in the absence of dislocations, i.e., the Burgers vector flux can be induced through the elastic

loading on the boundaries, even in a defect-free medium. This is appropriate on engineering length scales above or around a micron, where statistically stored dislocation (SSD) dominates the plastic deformation. (Methods to incorporate their effects into a theory like ours have been provided by Acharya *et al.* [8, 32] and Varadhan *et al.* [33])

By ignoring the SSDs, our theory assumes that there is an intermediate coarse-graining length scale, large compared to the distance between dislocations and small compared to the distance where the cancelling of dislocations with different Burger's vectors dominates the dynamics. We believe this latter length scale is given by the distance between cell walls (as discussed in Sec. 5.5). The cell wall misorientations are geometrically necessary, and we know of no experimental evidence that there are important numbers of the geometrically unnecessary SSDs inside cells. On the one hand, it is known [34, 35] that neighboring cell walls often have misorientations of alternating signs, so that on coarse-grained length scales just above the cell wall separation one would expect explicit treatment of the SSDs would be necessary. On the other hand, the density of dislocations in cell walls is high, so that a coarse-graining length much smaller than the interesting structures (and hence where we believe SSDs are unimportant) should be possible. (Our cell structures are fractal, with no characteristic 'cell size'; this coarse-graining length sets the minimum cutoff scale of the fractal, and the grain size or inhomogeneity length will set the maximum scale.) With this assumption, to treat the formation of cellular structures, we turn to theories of the form given in Eq. (2.15), defined in terms of dislocation currents J that depend directly on the local GND density.

2.5 Our CDD model

The microscopic motion of a dislocation under external strain depends upon temperature. In general, it moves quickly along the glide direction, and slowly (or not at all) along the climb direction where vacancy diffusion must carry away the atoms. The glide speed can be limited by phonon drag at higher temperatures, or can accelerate to nearly the speed of sound at low temperatures [36]. It is traditional to assume that the dislocation velocity is over-damped, and proportional to the component of the force per unit dislocation length in the glide plane.

To coarse-grain this microscopics, for reasons described above, we choose a CDD model whose dislocation currents vanish when the GND density vanishes. Limkumnerd and Sethna [6] derived a dislocation current J for this case using a closure approximation of the underlying microscopics. Their work reproduced (in the case of both glide and climb) an earlier dynamical model proposed by Acharya and collaborators [2, 5] assuming a single velocity field for the dislocations.

In our CGD and GOD-LVP dynamics (Sections 2.5.1 and 2.5.3 below), we also assume that all dislocations in the infinitesimal volume at $\mathbf{x}$ are moving with a common velocity $\boldsymbol{v}(\mathbf{x})$. This common velocity ansatz was first mentioned by Mura [37], but as a warning that it is an incorrect assumption. Microscopically, different dislocations in a region experience Peach-Koehler forces in different directions, and will not move in tandem. Indeed, it is the difference in velocities for dislocations on different slip systems that leads to entanglement. It is also not justified in a coarse-grained theory (unlike fluid mechanics, where momentum conservation and Galilean invariance leads to an emergent collective local velocity for systems in local equilibrium). However, we shall see that variants of the local velocity ansatz allow one to construct physically sensible 'model

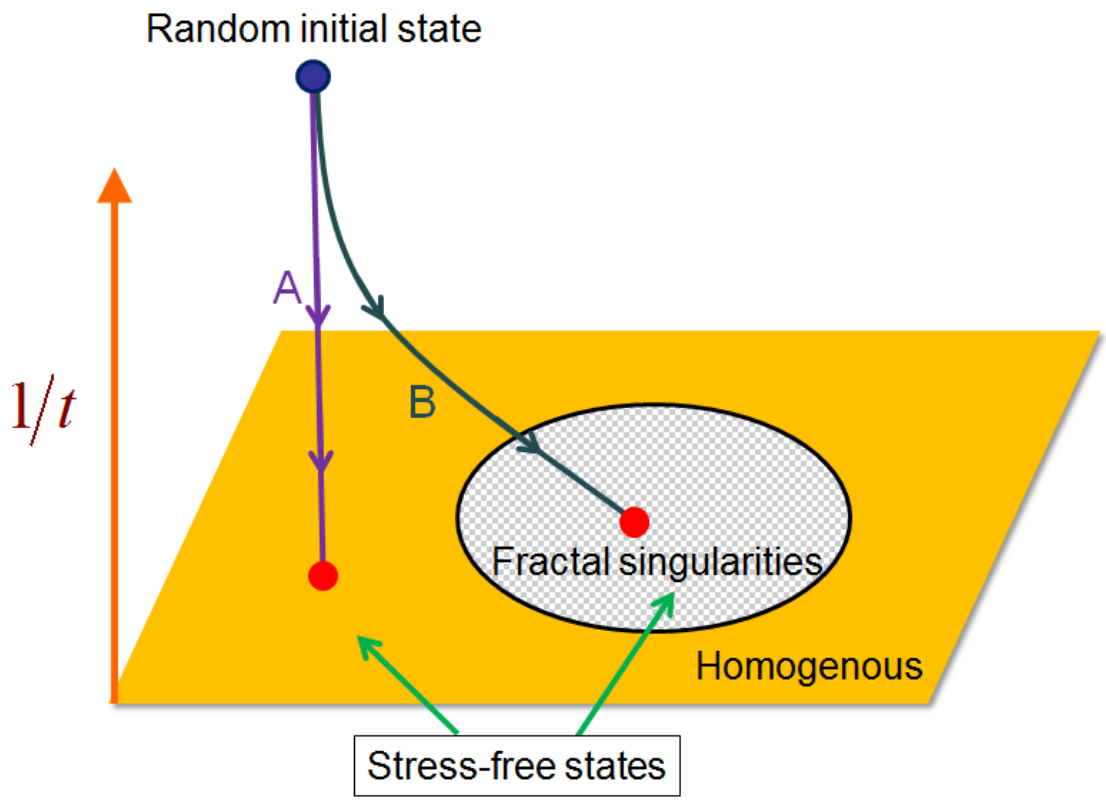

Figure 2.2: **Relaxation of various CDD models.** The blue dot represents the initial random plastically-deformed state; the red dots indicate the equilibrated stress-free states driven by different dynamics. Curve A: steepest decent dynamics leads to the trivial homogeneous equilibrated state, discussed in Sec. 2.4. Curve B: our continuum dislocation dynamics settles the system into non-trivial stress-free states with wall-like singularities of the GND density, discussed in Sec. 2.5.

materials' – perhaps not the correct theory for a particular material, but a sensible framework to generate theories of plastic deformation. This ansatz has been supplemented by constitutive laws for the velocity field by Acharya [2] and collaborators [3–5, 8, 33] to generate CDD theories. We follow their argument in Sec. 2.5.1 to derive the dynamics allowing both glide and climb, and then modify it to remove climb in Sec. 2.5.2. We also derive a second variant version of glide-only dynamics in Sec. 2.5.3 by approaching the limit of infinite vacancy energy, which reproduces a model proposed by Acharya and Roy [8].

2.5.1 Climb and glide dynamics (CGD)

We start with a model presuming (perhaps unphysically) that vacancy diffusion is so fast that dislocations climb and glide with equal mobility. The elastic Peach-Koehler force due to the stress $\sigma(\mathbf{x})$ on the local GND density is given by $f_u^{PK} = \sigma_{mk}\varrho_{umk}$. We assume that the velocity $\boldsymbol{v} \propto \boldsymbol{f}^{PK}$, giving a local constitutive relation

$$v_u \propto \sigma_{mk}\varrho_{umk}. \tag{2.40}$$

How should we determine the proportionality constant between velocity and force? In experimental systems, this is complicated by dislocation entanglement and short-range forces between dislocations. Ignoring these features, the velocity of each dislocation should depend only on the stress induced by the other dislocations, not the local density of dislocations [38]. We can incorporate this in an approximate way by making the proportionality factor in Eq. (2.40) inversely proportional to the GND density. We measure the latter by summing the square of all components of ϱ, hence $|\varrho| = \sqrt{\varrho_{ijk}\varrho_{ijk}/2}$ and $v_u = \frac{D}{|\varrho|}\sigma_{mk}\varrho_{umk}$, where D is a positive material-dependent constant. This choice has the additional important feature that the evolution of a sharp domain wall whose width is limited by the lattice cutoff is unchanged when the lattice cutoff is reduced.

The flux J of the Burgers vector is thus

$$J_{ij} = v_u\varrho_{uij} = \frac{D}{|\varrho|}\sigma_{mk}\varrho_{umk}\varrho_{uij}. \tag{2.41}$$

Notice that this dynamics satisfies our criterion that $J = 0$ when there are no GNDs (i.e., $\varrho = 0$).

Substituting this flux J (Eq. (2.41)) into the free energy dissipation rate (Eq. (C.6)) gives

$$\frac{\partial\mathcal{F}}{\partial t} = -\int d^3\mathbf{x}\ \sigma_{ij}J_{ij} = -\int d^3\mathbf{x}\ \frac{|\varrho|}{D}v^2 \leq 0. \tag{2.42}$$

Details are given in Appendix C.

2.5.2 Glide-only dynamics: mobile dislocation population (GOD-MDP)

When the temperature is low enough, dislocation climb is negligible, i.e., dislocations can only move in their glide planes. Fundamentally, dislocation glide conserves the total number of atoms, which leads to an unchanged local volume. Since the local volume change in time is represented by the trace J_{ii} of the flux of the Burgers vector, conservative motion of GNDs demands $J_{ii} = 0$. Limkumnerd and Sethna [6] derived the equation of motion for dislocation glide only, by removing the trace of J from Eq. (2.41). However, their dynamics fails to guarantee that the free energy monotonically decreases. Here we present an alternative approach.

We can remove the trace of J by modifying the first equality in Eq. (2.41),

$$J'_{ij} = v'_u\left(\varrho_{uij} - \frac{1}{3}\delta_{ij}\varrho_{ukk}\right), \tag{2.43}$$

where $\varrho'_{uij} = \varrho_{uij} - \frac{1}{3}\delta_{ij}\varrho_{ukk}$ can be viewed as a subset of 'mobile' dislocations moving with velocity $\boldsymbol{v}'$.

Substituting the flux (Eq. (2.43)) into the free energy dissipation rate (Eq. (C.6)) gives

$$\frac{\partial \mathcal{F}}{\partial t} = -\int d^3\mathbf{x}\ \sigma_{ij}(v'_u\varrho'_{uij}). \tag{2.44}$$

If we choose the velocity $v'_u \propto \sigma_{ij}\varrho'_{uij}$, the appropriate free energy monotonically decreases in time. We thus express $v'_u = \frac{D}{|\varrho|}\varrho'_{uij}\sigma_{ij}$, where D is a positive material-dependent constant, and the prefactor $1/|\varrho|$ is added for the same reasons, as discussed in the second paragraph of Sec. 2.5.1.

The flux J' of the Burgers vector is thus written [7]

$$J'_{ij} = v'_u \varrho'_{uij} = \frac{D}{|\varrho|}\sigma_{mn}\Big(\varrho_{umn} - \frac{1}{3}\delta_{mn}\varrho_{ull}\Big)\Big(\varrho_{uij} - \frac{1}{3}\delta_{ij}\varrho_{ukk}\Big). \tag{2.45}$$

This natural evolution law becomes much less self-evident when expressed in terms of the traditional two-index version ρ (Eqs. 2.1&2.2)

$$\begin{aligned} J'_{ij} \;=\; & \frac{D}{|\varrho|}\Big[\sigma_{in}\rho_{mn}\rho_{mj} - \sigma_{mn}\rho_{in}\rho_{mj} - \frac{1}{3}\sigma_{mm}\rho_{ni}\rho_{nj} + \frac{1}{3}\sigma_{mm}\rho_{in}\rho_{nj} \\ & -\frac{\delta_{ij}}{3}\Big(\sigma_{kn}\rho_{mn}\rho_{mk} - \sigma_{mn}\rho_{kn}\rho_{mk} - \frac{1}{3}\sigma_{mm}\rho_{nk}\rho_{nk} + \frac{1}{3}\sigma_{mm}\rho_{kn}\rho_{nk}\Big)\Big], \end{aligned} \tag{2.46}$$

(which is why we introduce the three-index variant ϱ).

This flux J' makes the free energy dissipation rate the negative of a perfect square in Eq. (C.8). Details are given in Appendix C.

2.5.3 Glide-only dynamics: local vacancy-induced pressure (GOD-LVP)

At high temperature, the fast vacancy diffusion leads to dislocation climb out of the glide direction. As the temperature decreases, vacancies are frozen out so that dislocations only slip in the glide planes. In Appendix 2.6, we present a dynamical model coupling the vacancy diffusion to our CDD model. Here we consider the limit of frozen-out vacancies with infinite energy costs, which leads to another version of glide-only dynamics.

According to the coupling dynamics Eq. (2.58), we write down the general form of dislocation current

$$J''_{ij} = \frac{D}{|\varrho|}\Big(\sigma_{mn} - \delta_{mn}p\Big)\varrho_{umn}\varrho_{uij}, \tag{2.47}$$

where p is the local pressure due to vacancies.

The limit of infinitely costly vacancies ($\alpha \to \infty$ in Appendix 2.6) leads to the traceless current, $J''_{ii} = 0$. Solving this equation gives a critical local pressure p^c

$$p^c = \frac{\sigma_{pq}\varrho_{spq}\varrho_{skk}}{\varrho_{uaa}\varrho_{ubb}}. \tag{2.48}$$

The corresponding current J'' of the Burgers vector in this limit is thus written

$$J''_{ij} = \frac{D}{|\varrho|}\Big(\sigma_{mn} - \frac{\sigma_{pq}\varrho_{spq}\varrho_{skk}}{\varrho_{uaa}\varrho_{ubb}}\delta_{mn}\Big)\varrho_{umn}\varrho_{uij}, \tag{2.49}$$

reproducing the glide-only dynamics proposed by Acharya and Roy [8].

Substituting the current (Eq. (2.49)) into the free energy dissipation rate (Eq. (C.6)) gives

$$\frac{\partial \mathcal{F}}{\partial t} = -\int d^3\mathbf{x}\frac{D}{|\varrho|}\Big[(f_i^{PK}f_i^{PK} - \Big(\frac{d_i f_i^{PK}}{|\mathbf{d}|}\Big)^2\Big] \leq 0, \tag{2.50}$$

where $f_i^{PK} = \sigma_{mn}\varrho_{imn}$ and $d_i = \varrho_{ikk}$. The equality emerges when the force $\mathbf{f}^{PK}$ is along the same direction as $\mathbf{d}$.

Unlike the traditional linear dissipative models, our CDD model, coarse grained from microscopic interactions, drives the random plastic distortion to non-trivial stress-free states with dislocation wall singularities, as schematically illustrated in Fig. 2.2.

Our minimal CDD model, consisting of GNDs evolving under the long-range interaction, provides a framework for understanding dislocation morphologies at the mesoscale. Eventually, it can be extended to include vacancies by coupling them to the dislocation current (as discussed in Appendix 2.6, or extended to include disorder, dislocation pinning, and entanglement by adding appropriate interactions to the free energy functional and refining the effective stress field (as discussed in Appendix 2.8). It has already been extended to include SSDs incorporating traditional crystal plasticity theories [8, 32, 33].

2.6 Coupling to vacancies

In plastically deformed crystals at low temperature, dislocations usually move only in the glide plane because vacancy diffusion is almost frozen out. When temperature increases, vacancy diffusion leads to dislocation climb out of the glide plane. At intermediate temperatures, slow vacancy diffusion can enable local creep. The resulting dynamics should couple the vacancy and dislocation fields in non-trivial ways. Here we couple the vacancy diffusion to the dislocation motion in our CDD model.

We introduce an order parameter field $c(\mathbf{x})$, indicating the vacancy concentration density at the point $\mathbf{x}$. The free energy $\mathcal{F}$ is thus expressed

$$\mathcal{F} = \mathcal{F}^{Dis} + \mathcal{F}^{Vac} = \int d^3\mathbf{x}\Big(\frac{1}{2}\sigma_{ij}\epsilon^{\mathrm{e}}_{ij} + \frac{1}{2}\alpha(c - c_0)^2\Big), \tag{2.51}$$

where α is a positive material parameter related to the vacancy creation energy, and c_0 is the overall equilibrium vacancy concentration density.

Assuming that GNDs share the velocity $\boldsymbol{v}$ in an infinitesimal volume, we write the current J for GNDs

$$J_{ij} = v_u \varrho_{uij}. \tag{2.52}$$

The current trace J_{ii} describes the rate of volume change, which acts as a source and sink of vacancies. The coupling dynamics for vacancies is thus given

$$\partial_t c = \gamma \nabla^2 c + J_{ii}, \tag{2.53}$$

where γ is a positive vacancy diffusion constant.

The infinitesimal change of the free energy $\mathcal{F}$ (Eq. (2.51)) is

$$\delta\mathcal{F} = \int d^3\mathbf{x}\Big(\frac{\delta\mathcal{F}^{Dis}}{\delta\beta^{\mathrm{p}}_{ij}}\delta\beta^{\mathrm{p}}_{ij} + \frac{\delta\mathcal{F}^{Vac}}{\delta c}\delta c\Big). \tag{2.54}$$

We apply Eq. (C.5) and $\delta\mathcal{F}^{Vac}/\delta c = \alpha(c - c_0)$

$$\delta\mathcal{F} = \int d^3\mathbf{x}\Big(-\sigma_{ij}\delta\beta^{\mathrm{p}}_{ij} + \alpha(c - c_0)\delta c\Big). \tag{2.55}$$

The free energy dissipation rate is thus $\delta\mathcal{F}/\delta t$ for $\delta\beta^{\mathrm{p}}_{ij} = \frac{\partial\beta^{\mathrm{p}}}{\partial t}\delta t$ and $\delta c = \frac{\partial c}{\partial t}\delta c$, hence

$$\frac{\partial\mathcal{F}}{\partial t} = -\int d^3\mathbf{x}\Big(\sigma_{ij}\frac{\partial\beta^{\mathrm{p}}_{ij}}{\partial t} - \alpha(c - c_0)\frac{\partial c}{\partial t}\Big). \tag{2.56}$$

Substituting the current J (Eq. (2.52)) and Eq. (2.53) into Eq. (2.56) gives

$$\begin{aligned}\frac{\partial\mathcal{F}}{\partial t} &= -\int d^3\mathbf{x}(\sigma_{ij}(v_u\varrho_{uij}) - \alpha(c - c_0)(\gamma\nabla^2 c + v_u\varrho_{uii})) \\ &= -\int d^3\mathbf{x}((\sigma_{ij} - \alpha(c - c_0)\delta_{ij})\varrho_{uij})v_u - \int d^3\mathbf{x}\alpha\gamma(\nabla c)^2,\end{aligned} \tag{2.57}$$

where we integrate by parts by assuming an infinitely large system.

If we choose the velocity $v_u = \frac{D}{|\varrho|}(\sigma_{ij} - \alpha(c - c_0)\delta_{ij})\varrho_{uij}$, ($D$ is a positive material dependent constant and $1/|\varrho|$ is added for the same reasons as discussed in Sec. 2.5.1), the free energy is guaranteed to decrease monotonically. The coupling dynamics for both GNDs and vacancies is thus

$$\begin{cases} \partial_t\beta^{\mathrm{p}}_{ij} = \frac{D}{|\varrho|}(\sigma_{mn} - \alpha(c - c_0)\delta_{mn})\varrho_{umn}\varrho_{uij}, \\ \partial_t c = \gamma\nabla^2 c + \frac{D}{|\varrho|}(\sigma_{mn} - \alpha(c - c_0)\delta_{mn})\varrho_{umn}\varrho_{ukk}. \end{cases} \tag{2.58}$$

This dynamics gives us a clear picture of the underlying physical mechanism: the vacancies contribute an extra hydrostatic pressure $p = -\alpha(c - c_0)$.

2.7 Incorporating slip systems

When real crystals deform under tension or shear loading, plastic deformation usually occurs by slip on a particular set of crystallographic planes, known as slip planes. In

addition, slip always takes place along a consistent set of directions within these planes, called slip directions. The combination of slip plane and slip direction together makes up a slip system. These important realistic features have been studied by Koslowski *et al.* [39, 40], Arsenlis *et al.* [41, 42], etc. Here, we show how to incorporate them in an alternative CDD model.

Instead of the plastic distortion β^{p} or the GND density ρ, we use the local shear strain $\gamma^{(\alpha)}$ as the order parameter field, which evolves in the α-th slip system. All physical quantities, like β^{p}, ρ, and σ, can be fully specified in terms of γ.

A crystal structure can be described by the slip systems. For instance, there are 12 for FCC crystals, 24 or 48 for BCC crystals. Every slip system is defined by the slip plane normal direction $\hat{\mathbf{n}}$ and the slip direction $\hat{\mathbf{b}}$ (the direction of Burgers vector). The plastic distortion field β^{p} can be described by the sum of local shear strains over all slip systems

$$\beta^{\mathrm{p}}_{ij}(\mathbf{x}) = \sum_{\alpha} \gamma^{(\alpha)}(\mathbf{x}) \hat{n}^{(\alpha)}_{i} \hat{b}^{(\alpha)}_{j}, \tag{2.59}$$

where α indicates the α-th slip system, and $\gamma^{(\alpha)}$ is the local shear strain in this slip system.

The GND density tensor ρ can be written in terms of the sum of projection dislocation density tensors $\hat{\rho}$ over all slip systems

$$\rho_{ij}(\mathbf{x}) = \sum_{\alpha} \hat{\rho}^{(\alpha)}_{ij}(\mathbf{x}). \tag{2.60}$$

Substituting Eq. (2.59) into the relation (Eq. (2.9)) between β^{p} and ρ gives

$$\rho_{ij} = -\epsilon_{ilm} \partial_l \Big(\sum_{\alpha} \gamma^{(\alpha)} \hat{n}^{(\alpha)}_{m} \hat{b}^{(\alpha)}_{j} \Big). \tag{2.61}$$

Comparing Eq. (2.60) and Eq. (2.61) gives the projection dislocation density tensor $\hat{\rho}^{(\alpha)}$ in the α-th slip systems

$$\hat{\rho}^{(\alpha)}_{ij} = -\epsilon_{ilm} \partial_l \gamma^{(\alpha)} \hat{n}^{(\alpha)}_{m} \hat{b}^{(\alpha)}_{j}. \tag{2.62}$$

And the net projection dislocation density $|\hat{\rho}^{(\alpha)}|$ is given

$$|\hat{\rho}^{(\alpha)}| = \sqrt{\hat{\rho}^{(\alpha)}_{ij}\hat{\rho}^{(\alpha)}_{ij}} = \sqrt{\partial_l\gamma^{(\alpha)}\partial_l\gamma^{(\alpha)} - \hat{n}^{(\alpha)}_l\partial_l\gamma^{(\alpha)}\hat{n}^{(\alpha)}_m\partial_m\gamma^{(\alpha)}}. \tag{2.63}$$

The internal stress field σ projected into the α-th slip system gives the resolved shear stress τ

$$\tau^{(\alpha)} = \sigma_{ij}\hat{n}^{(\alpha)}_i\hat{b}^{(\alpha)}_j. \tag{2.64}$$

The Burgers vector flux J can be defined as

$$J_{ij} = \sum_\alpha j^{(\alpha)}_{ij} = \sum_\alpha j^{(\alpha)}\hat{n}^{(\alpha)}_i\hat{b}^{(\alpha)}_j, \tag{2.65}$$

where $j^{(\alpha)}$ is a net measure of the projection Burgers vector flux tensor $j^{(\alpha)}_{ij}$ in the α-th slip system,

$$j^{(\alpha)} = j^{(\alpha)}_{ij}\hat{n}^{(\alpha)}_i\hat{b}^{(\alpha)}_j. \tag{2.66}$$

The conservation law of Burgers vectors in every slip system is thus written

$$\frac{\partial\hat{\rho}^{(\alpha)}_{ij}}{\partial t} = -\epsilon_{ilm}\partial_l j^{(\alpha)}_{mj} = -\epsilon_{ilm}\partial_l j^{(\alpha)}\hat{n}^{(\alpha)}_m\hat{b}^{(\alpha)}_j. \tag{2.67}$$

The time evolution law of the plastic distortion is written

$$\frac{\partial}{\partial t}\beta^{\mathrm{p}}_{ij} = \sum_\alpha \frac{\partial\gamma^{(\alpha)}}{\partial t}\hat{n}^{(\alpha)}_i\hat{b}^{(\alpha)}_j = J_{ij}. \tag{2.68}$$

Comparing Eq. (2.65) and Eq. (2.68) gives the time evolution law of the local shear strain

$$\frac{\partial}{\partial t}\gamma^{(\alpha)} = j^{(\alpha)}. \tag{2.69}$$

The net projection Burgers vector flux $j^{(\alpha)}$ is driven by the resolved shear stress on the projection GND density $\hat{\rho}^{(\alpha)}$

$$j^{(\alpha)} = D\tau^{(\alpha)}|\hat{\rho}^{(\alpha)}|, \tag{2.70}$$

where D is a positive materials constant.

We can also derive the net projection Burgers vector flux in an intuitive way. We start from the Peach-Koehler force $\mathbf{f}^{PK}$ on the local projection GND density tensor $\hat{\rho}^{(\alpha)}$

$$f_i^{PK} = \epsilon_{iqp}\hat{\rho}_{ph}^{(\alpha)}\sigma_{qh}. \tag{2.71}$$

Substituting Eq. (2.62) into Eq. (2.71) gives

$$f_i^{PK} = \partial_q\gamma^{(\alpha)}\hat{n}_i^{(\alpha)}\hat{b}_h^{(\alpha)}\sigma_{qh} - \partial_i\gamma^{(\alpha)}\tau^{(\alpha)} \tag{2.72}$$

Enforcing the Peach-Koehler force in the slip system gives

$$f_i^{(\alpha)} = f_i^{PK} - (\hat{n}_j^{(\alpha)}f_j^{PK})\hat{n}_i^{(\alpha)}. \tag{2.73}$$

Substituting Eq. (2.71) into Eq. (2.73) gives

$$f_i^{(\alpha)} = \left(\hat{n}_i^{(\alpha)}\hat{n}_j^{(\alpha)}\partial_j\gamma^{(\alpha)} - \partial_i\gamma^{(\alpha)}\right)\tau^{(\alpha)}. \tag{2.74}$$

Since the flow of the projection GNDs can be characterized by a single velocity $\mathbf{v}$, which is proportional to the projection Peach-Kohler force $\mathbf{f}^{(\alpha)}$, we define

$$v_i^{(\alpha)} = \frac{D}{|\hat{\rho}^{(\alpha)}|}f_i^{(\alpha)}, \tag{2.75}$$

where we use the prefactor $1/|\hat{\rho}^{(\alpha)}|$ motivated by the same considerations as in Sec. 2.5.

The projection Burgers vector flux tensor $j_{ij}^{(\alpha)}$ is expressed

$$j_{ij}^{(\alpha)} = \epsilon_{lim}v_l^{(\alpha)}\hat{\rho}_{mj}^{(\alpha)}. \tag{2.76}$$

Substituting Eqs. (2.62) and (2.75) into Eq. (2.76) and applying Eq. (2.66) gives

$$\begin{aligned} j^{(\alpha)} &= \frac{D}{|\hat{\rho}^{(\alpha)}|}\epsilon_{lim}f_l^{(\alpha)}\left(-\epsilon_{msq}\partial_s\gamma^{(\alpha)}\hat{n}_q^{(\alpha)}\hat{b}_j^{(\alpha)}\right)\hat{n}_i^{(\alpha)}\hat{b}_j^{(\alpha)} \\ &= \frac{D\tau^{(\alpha)}}{|\hat{\rho}^{(\alpha)}|}\left(\partial_l\gamma^{(\alpha)}\partial_l\gamma^{(\alpha)} - \hat{n}_l^{(\alpha)}\partial_l\gamma^{(\alpha)}\hat{n}_j^{(\alpha)}\partial_j\gamma^{(\alpha)}\right) \\ &= D\tau^{(\alpha)}|\hat{\rho}^{(\alpha)}|. \end{aligned} \tag{2.77}$$

This net projection Burgers vector flux $j^{(\alpha)}$ is exactly the same as Eq. (2.70).

When turning on the external loading, the net projection Burgers vector flux $j^{(\alpha)}$ is written

$$j^{(\alpha)} = D(\tau^{(\alpha)} + \tau_{ext}^{(\alpha)})|\hat{\rho}^{(\alpha)}|, \tag{2.78}$$

where $\tau_{ext}^{(\alpha)}$ is the projection external stress in the α-th slip system, $\tau_{ext}^{(\alpha)} = \sigma_{ij}^{ext}\hat{n}_i^{(\alpha)}\hat{b}_j^{(\alpha)}$.

Due to the dissipative nature of dislocation motion, this dislocation dynamics needs to yield monotonically decreasing the appropriate free energy. We can check this. Substituting Eq. (2.68) into the free energy dissipation rate Eq. (C.6) gives

$$\begin{aligned} \frac{\partial \mathcal{F}}{\partial t} &= -\int (\sigma_{ij}^{int} + \sigma_{ij}^{ext}) \sum_{\alpha} \Big(\frac{\partial \gamma^{(\alpha)}}{\partial t} \hat{n}_i^{(\alpha)} \hat{b}_j^{(\alpha)} \Big) dV \\ &= -\sum_{\alpha} \int \Big(\tau^{(\alpha)} + \tau_{ext}^{(\alpha)} \Big) \frac{\partial \gamma^{(\alpha)}}{\partial t} dV. \end{aligned} \tag{2.79}$$

Substituting Eq. (2.70) into Eq. (2.79) gives

$$\frac{\partial \mathcal{F}}{\partial t} = -\sum_{\alpha} \int D\Big(\tau^{(\alpha)} + \tau_{ext}^{(\alpha)} \Big)^2 |\hat{\rho}^{(\alpha)}| dV \leq 0. \tag{2.80}$$

which implies that the free energy decreases with time monotonically.

2.8 Coupling to disorder

In real crystals, the presence of precipitates or impurities results in a force pinning nearby dislocations. We can mimic this effect by incorporating a spatially varying random potential field $V(\mathbf{x})$.

In our CDD model, we can add the interaction energy between GNDs and random disorder into the free energy $\mathcal{F}$ (Eq. (2.25))

$$\mathcal{F} = \mathcal{F}_E + \mathcal{F}_I = \int d^3\mathbf{x} \Big(\frac{1}{2} \sigma_{ij}^{\text{int}} \epsilon_{ij}^{\text{e}} - \sigma_{ij}^{\text{ext}} \epsilon_{ij}^{\text{p}} + V(\mathbf{x}) |\varrho| \Big), \tag{2.81}$$

where $\mathcal{F}_E$ indicates the elastic free energy corresponding to the integral of the first two terms, and $\mathcal{F}_I$ indicates the interaction energy, the integral of the last term.

An infinitesimal change of the free energy is written

$$\delta\mathcal{F} = \delta\mathcal{F}_E + \delta\mathcal{F}_I = \int d^3\mathbf{x}\Big(\frac{\delta\mathcal{F}_E}{\delta\beta^{\mathrm{p}}_{ij}}\delta\beta^{\mathrm{p}}_{ij} + \frac{\delta\mathcal{F}_I}{\delta\beta^{\mathrm{p}}_{sk}}\delta\beta^{\mathrm{p}}_{sk}\Big). \tag{2.82}$$

In an infinitely large system, Eq. (C.5) gives

$$\frac{\delta\mathcal{F}_E}{\delta\beta^{\mathrm{p}}_{ij}} = -(\sigma^{\mathrm{int}}_{ij} + \sigma^{\mathrm{ext}}_{ij}), \tag{2.83}$$

and Eq. (B.2) implies

$$\begin{aligned}\delta\mathcal{F}_I &= \int d^3\mathbf{x} g_{ijls}\partial_l\Big(\frac{\delta\mathcal{F}_I}{\delta\varrho_{ijk}}\Big)\delta\beta^{\mathrm{p}}_{sk} \\ &= \int d^3\mathbf{x} g_{ijls}\partial_l\Big(V(\mathbf{x})\frac{\varrho_{ijk}}{|\varrho|}\Big)\delta\beta^{\mathrm{p}}_{sk}.\end{aligned} \tag{2.84}$$

Substituting Eq. (2.83) and Eq. (2.84) into Eq. (2.82) gives

$$\begin{aligned}\delta\mathcal{F} &= -\int d^3\mathbf{x}\Big(\sigma^{\mathrm{int}}_{ij} + \sigma^{\mathrm{ext}}_{ij} - g_{mnli}\partial_l\Big(V(\mathbf{x})\frac{\varrho_{mnj}}{|\varrho|}\Big)\Big)\delta\beta^{\mathrm{p}}_{ij} \\ &= -\int d^3\mathbf{x}\sigma^{\mathrm{eff}}_{ij}\delta\beta^{\mathrm{p}}_{ij}.\end{aligned} \tag{2.85}$$

where the effective stress field is $\sigma^{\mathrm{eff}}_{ij} = \sigma^{\mathrm{int}}_{ij} + \sigma^{\mathrm{ext}}_{ij} - g_{mnli}\partial_l\Big(V(\mathbf{x})\frac{\varrho_{mnj}}{|\varrho|}\Big)$.

By replacing σ with σ^{eff} in the equation of motion of either allowing climb (Eq. (2.41)) or removing climb (Eq. (2.45)), we achieve a new CDD model that models GNDs interacting with disorder.

CHAPTER 3

SIMULATIONS[1]

3.1 Introduction

We perform simulations in 2D and 3D the dislocation dynamics of Eq. (2.15) and Eq. (2.18), with dynamical currents defined by climb and glide dynamics (CGD) (Eq. 2.41), glide-only dynamics due to mobile dislocation population (GOD-MDP) (Eq. 2.45), and glide-only dynamics due to local vacancy pressure (GOD-LVP) (Eq. 2.49). The summary of dynamical equations are discussed in Appendix D. We numerically observe that simulations of Eqs. (2.15), (2.18) lead to the same results statistically (i.e., the numerical time step approximations leave the physics invariant). We therefore focus our presentation on the results of Eq. (2.18), where the evolving field variable β^{p} is unconstrained. Our CGD and GOD-MDP models have been quite extensively simulated in one and two dimensions and relevant results can be found in Refs. [6], [43], and [7]. In this chapter, we concentrate on periodic grids of spatial extent L in both two [7] and three dimensions.

3.2 Methods

The numerical approach we use is a second order central upwind scheme designed for Hamilton-Jacobi equations [44] using finite differences. This method is quite efficient in capturing $\delta-$shock singular structures [45], even though it is flexible enough to allow for the use of approximate solvers near the singularities.

[1]This chapter is part of a preprint (arXiv:1106.0195) in collaboration with Woosong Choi, Stefanos Papanikolaou, Matthew Bierbaum, and James Sethna. This manuscript has been submitted to Physical Review B.

Our numerical simulations show a close analogy to those of turbulent flows [45]. As in three-dimensional turbulence, defect structures lead to intermittent transfer of morphology to short length scales. As conjectured [46, 47] for the Euler equations or the inviscid limit of Navier-Stokes equations, our simulations develop singularities in finite time [6, 7]. Here these singularities are δ-shocks representing grain-boundary-like structures emerging from the mutual interactions among mobile dislocations [48]. In the presence of artificial viscosity, our simulations exhibit nice numerical convergence in all dimensions [48]. However, in the limit of vanishing viscosity, the solutions of our dynamics continue to depend on the lattice cutoff in higher dimensions, (our simulations only exhibit numerical convergence in one dimension). Actually, the fact that the physical system is cut off by the atomic scale leads to the conjecture that our equations are in some sense non-renormalizable in the ultraviolet. These issues are discussed in detail in Refs. [45] and [48].

In the vanishing viscosity limit, our simulations exhibit fractal structure down to the smallest scales. When varying the system size continuously, the solutions of our dynamics exhibit a convergent set of correlation functions of the various order parameter fields, which are used to characterize the emergent self-similarity. This statistical convergence is numerically tested in Sec. 5.5.

3.3 Gaussian random initial conditions

Gaussian random fields are extensively used in physical modelings to mimic stochastic fluctuations with a correlated length scale. In our simulations, we construct an initially random plastic distortion, a nine-component tensor field, where every component is an independent Gaussian random field sharing an underlying length scale.

We define a Gaussian random field f with correlation length σ_0 by convolving white noise $\langle \xi(\mathbf{x})\xi(\mathbf{x}')\rangle = \delta(\mathbf{x}-\mathbf{x}')$ with a Gaussian of width σ_0:

$$f(\mathbf{x}) = \int d^3\mathbf{x}'\xi(\mathbf{x}')e^{-(\mathbf{x}-\mathbf{x}')^2/\sigma_0^2}. \tag{3.1}$$

In Fourier space, this can be done as a multiplication:

$$\widetilde{f}(\mathbf{k}) = e^{-\sigma_0^2 k^2/4}\widetilde{\xi}(\mathbf{k}). \tag{3.2}$$

The square $\widetilde{f}(\mathbf{k})\widetilde{f}(-\mathbf{k}) = e^{-\sigma_0^2 k^2/2}$ implies that the correlation function $\langle f(\mathbf{x})f(\mathbf{x}')\rangle = (2\pi\sigma_0^2)^{-3/2}e^{-(\mathbf{x}-\mathbf{x}')^2/(2\sigma_0^2)}$.

In our simulations, the initial plastic distortion tensor field β^{p} is constructed in Fourier space

$$\widetilde{\beta}^{\mathrm{p}}_{ij}(\mathbf{k}) = e^{-\sigma_0^2 k^2/4}\widetilde{\zeta}_{ij}(\mathbf{k}), \tag{3.3}$$

where the white noise signal ζ is characterized as $\langle \zeta_{(i,j)}(\mathbf{x})\zeta_{(i,j)}(\mathbf{x}')\rangle = A_{(i,j)}\delta(\mathbf{x}-\mathbf{x}')$, and in Fourier space $\frac{1}{V}\widetilde{\zeta}_{(i,j)}(\mathbf{k})\widetilde{\zeta}_{(i,j)}(-\mathbf{k}) = A_{(i,j)}$. (We use (i, j) to indicate a component of the tensor field, to avoid the Einstein summation rule.) The correlation function of each component of $\beta^{\mathrm{p,I}}$ is thus expressed in Fourier space

$$\begin{aligned}\widetilde{C}^{\beta^{\mathrm{p,I}}}_{(i,j)} &= 2\langle \beta^{\mathrm{p,I}}_{(i,j)}\beta^{\mathrm{p,I}}_{(i,j)}\rangle(2\pi)^3\delta(\mathbf{k}) - \frac{2}{V}\widetilde{\beta}^{\mathrm{p}}_{(i,j)}(\mathbf{k})\widetilde{\beta}^{\mathrm{p}}_{(i,j)}(-\mathbf{k}) \\ &= 2\langle \beta^{\mathrm{p,I}}_{(i,j)}\beta^{\mathrm{p,I}}_{(i,j)}\rangle(2\pi)^3\delta(\mathbf{k}) - 2A_{(i,j)}e^{-\sigma_0^2 k^2/2},\end{aligned} \tag{3.4}$$

where the Gaussian kernel width σ_0, as a standard length scale, defines the correlation length of our simulation. (In our earlier work, we use a non-standard definition for the correlation length, so our σ_0 equals the old length scale times $\sqrt{2}$.)

According to Eq. (2.9) and Eq. (3.3), we can express the initial GND density field ρ in Fourier space

$$\widetilde{\rho}_{ij}(\mathbf{k}) = -i\varepsilon_{ilm}e^{-\sigma_0^2 k^2/4}k_l\widetilde{\zeta}_{mj}(\mathbf{k}). \tag{3.5}$$

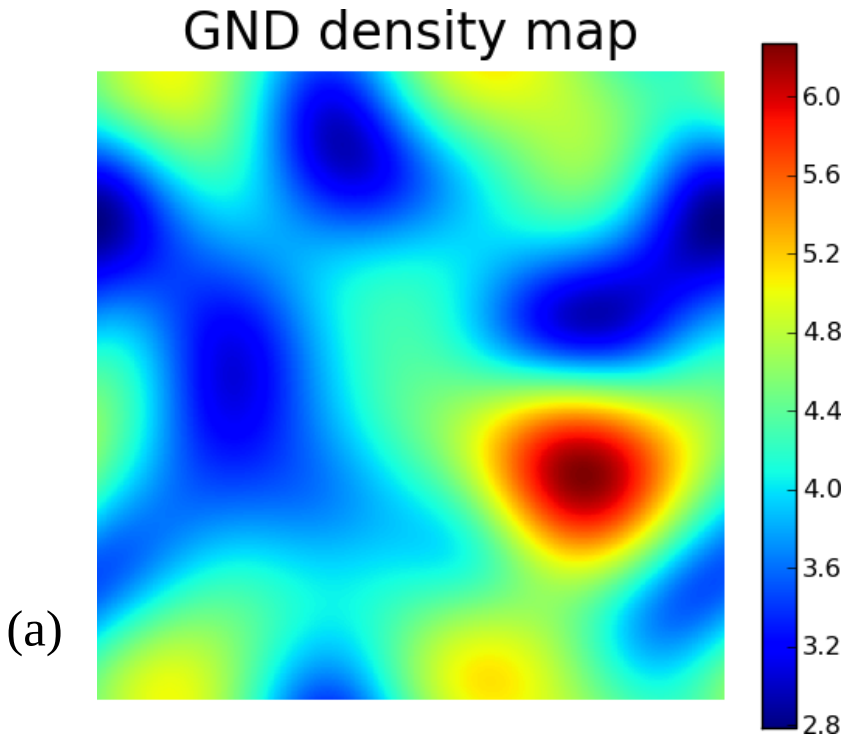

(a)

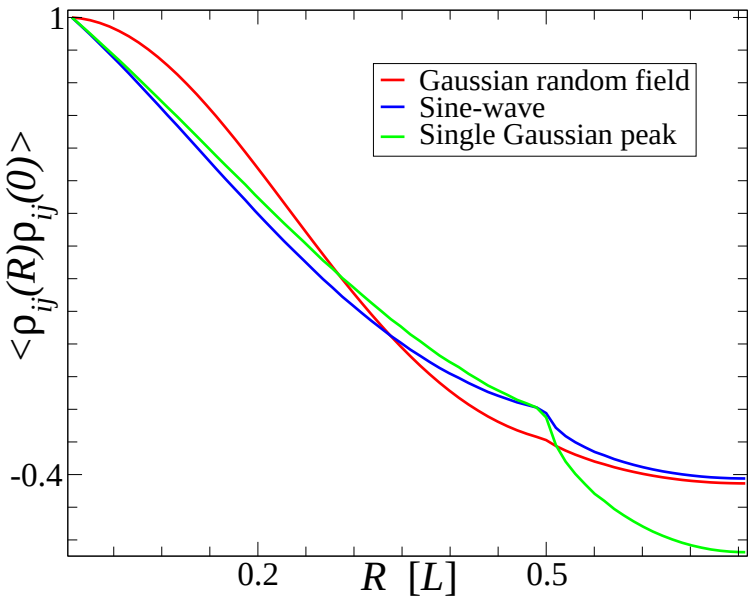

(b)

Figure 3.1: **Gaussian random initial conditions with the correlated length scale** $0.28L$ **in two dimensions.** (a) shows the initial net GND density map; (b) exhibits the correlation functions of ρ under various initial conditions, where we compare the Gaussian random field to both a sinusoidal wave and a single periodic superposition of Gaussian peaks. The kink arises due to the edges and corners of the square unit cell.

The scalar invariant C^{ρ}_{tot} of the correlation function of ρ is thus expressed in Fourier space

$$C^{\rho}_{tot}(\mathbf{k}) = \frac{1}{V}\widetilde{\rho}_{ij}(\mathbf{k})\widetilde{\rho}_{ij}(-\mathbf{k}) = \frac{1}{V}e^{-\sigma_0^2 k^2/2}(k^2\delta_{mn} - k_m k_n)\widetilde{\zeta}_{mj}(\mathbf{k})\widetilde{\zeta}_{nj}(-\mathbf{k}). \tag{3.6}$$

The resulting initial GND density is not Gaussian correlated, unlike the initial plastic distortion. Figure 3.1 exhibits the initial GND density map due to the Gaussian random plastic distortions with the correlation length $0.28L$, and its correlation function. We compare the latter to the correlation functions of both a sinusoidal wave and a single periodic superposition of Gaussian peaks. The similarity of the three curves shows that our Gaussian random initial condition at $\sigma_0 \sim 0.28L$ approaches the largest effective correlation length possible for periodic boundary conditions.

3.4 Two dimensional simulations

In two dimensional simulations, we relax the deformed system with and without dislocation climb in the absence of external loading. Here, the initial plastic distortion field β^{p} is still a Gaussian random field with correlation length scale $\sqrt{2}L/5 \sim 0.28L$ and initial amplitude $\beta_0 = 1$. (In our earlier work [7], we described this length as $L/5$, using a non-standard definition of correlation length scale; see Sec. 3.3.) These random initial conditions are explained in Sec. 3.3. In two dimensions, Figure 3.2 shows that CGD and GOD-LVP simulations (top and bottom) exhibit much sharper, flatter boundaries than GOD-MDP (middle). This difference is quantitatively described by the large shift in the static critical exponent η in two dimensions for both CGD and GOD-LVP. In our earlier work [7], we announced this difference as providing a sharp distinction between high-temperature, non-fractal grain boundaries (for CGD), and low-temperature, fractal cell wall structures (for GOD-MDP). During two dimensional relaxations, their appropriate

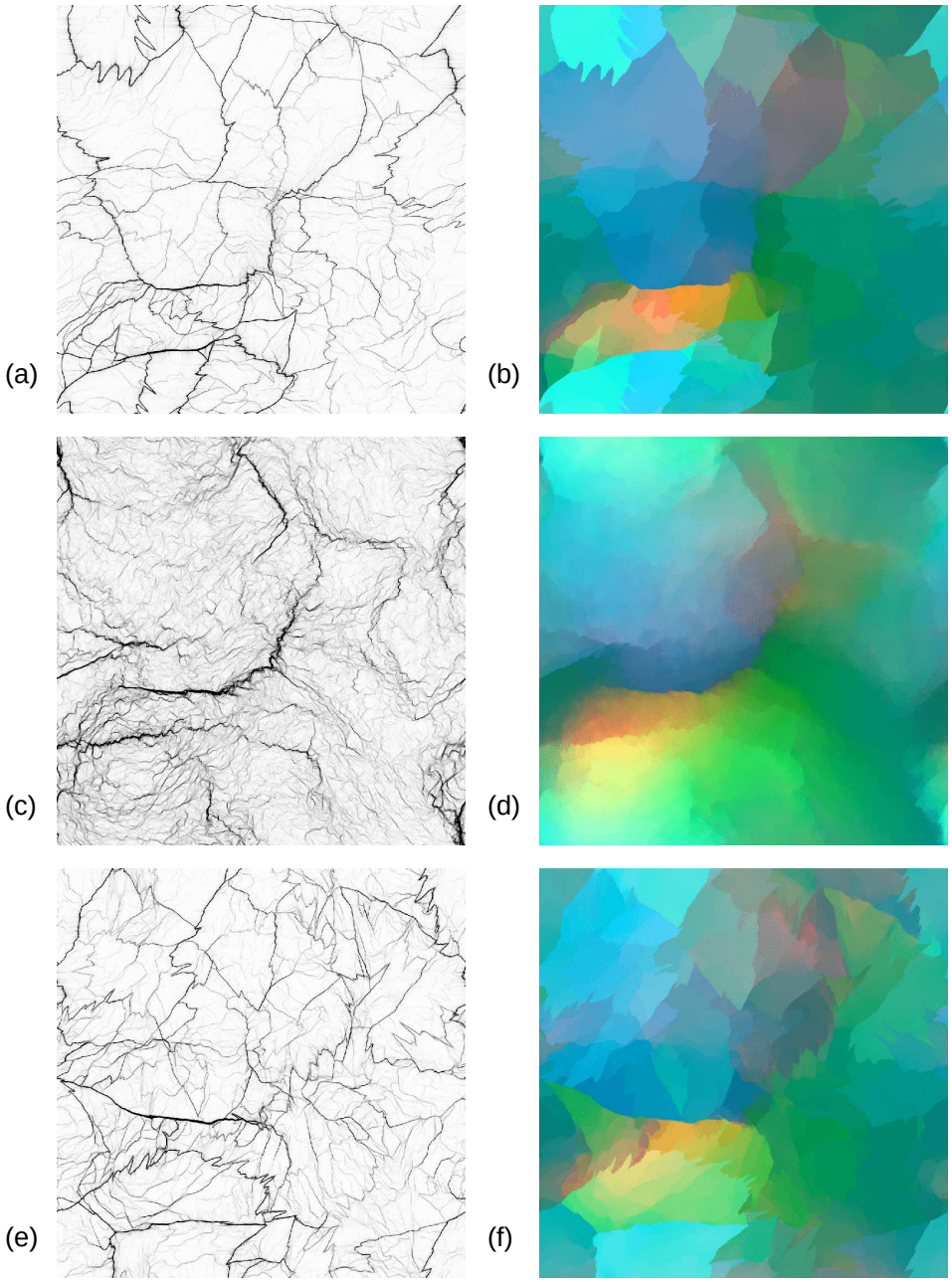

Figure 3.2: **Complex dislocation structures in two dimensions** (1024^2) for the relaxed states of an initially random distortion. *Top:* CGD; *Middle:* GOD-MDP; *Bottom:* GOD-LVP. *Left:* Net GND density $|\varrho|$ plotted linearly in density with dark regions a factor $\sim 10^4$ more dense than the lightest visible regions. (a) When climb is allowed, the resulting morphologies are sharp, regular, and close to the system scale. (c) When climb is forbidden using a mobile dislocation sub-population, there is a hierarchy of walls on a variety of length scales, getting weaker on finer length scales. (e) When climb is removed using a local vacancy pressure, the resulting morphologies are about as sharp as those (a) allowing climb. *Right:* Corresponding local crystalline orientation maps, with the three components of the orientation vector $\mathbf{\Lambda}$ linearly mapped onto a vector of RGB values. Notice the fuzzier cell walls (c) and (d) suggests a larger fractal dimension.

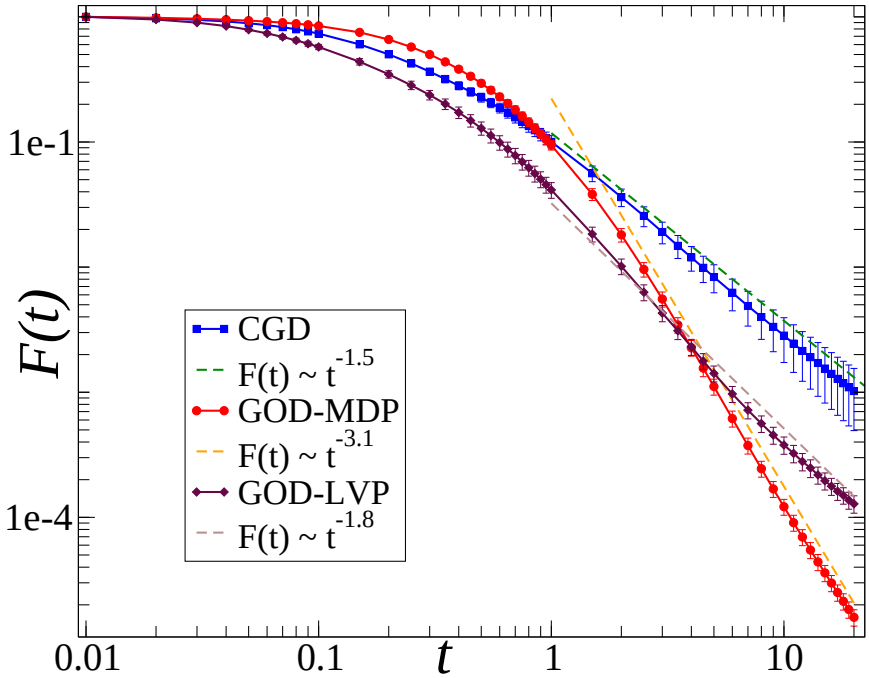

Figure 3.3: **The elastic free energy decreases to zero as a power law in time in two dimensions.** We show that the free energy $\mathcal{F}$ decays monotonically in time, and goes to zero as a power law for CGD, GOD-MDP, and GOD-LVP simulations, as the system relaxes in the absence of external strain.

free energies monotonically decay to zero as shown in Fig. 3.3.

After GNDs evolve into stress-free states, we exert anisotropic loadings on the system as performed in experiments. In two dimensions, we apply the uniaxial tension loadings both normal and parallel to the simulated system, schematically shown in Fig. 3.4(a) and (b). Along the axis of the uniaxial tension, we stretch the system with the strain rate $\dot{\epsilon} = 0.05\beta_0^2$ and squash it in the rest two orthogonal directions with half of the strain rate simultaneously. (In order to approach the quasi-static limit, we apply the strain rate as slowly as practical.) Figure 3.4 shows that simulations loaded normal to the two-dimensional system exhibit more isotropic fractal patterns than those loaded in the plane of the system.

Figure 3.4: Complex dislocation structures under anisotropic loadings in two dimensions (1024^2). In (a) and (b), we schematically show that the uniaxial tension loadings are applied both normal and parallel to the two-dimensional system. In both cases, we start from the well-relaxed system (shown in Fig. 3.2(b) and (d)) and exert uniaxial loading with a slow constant strain rate $\dot{\varepsilon} = 0.05\ \frac{\mu^2}{\mu_0}$. When the systems are loaded up to $\varepsilon = 3\ \varepsilon_0$, the net GND density maps ρ_{GND} are shown in (c) and (d), and the corresponding local crystalline maps shown in (e) and (f). The cellular structures ((c) and (e)) due to the out-of-plane loading seem more isotropic than those ((d) and (f)) due to the in-plane loading. Notice the horizontal and vertical directions corresponding to X and Y axes respectively.

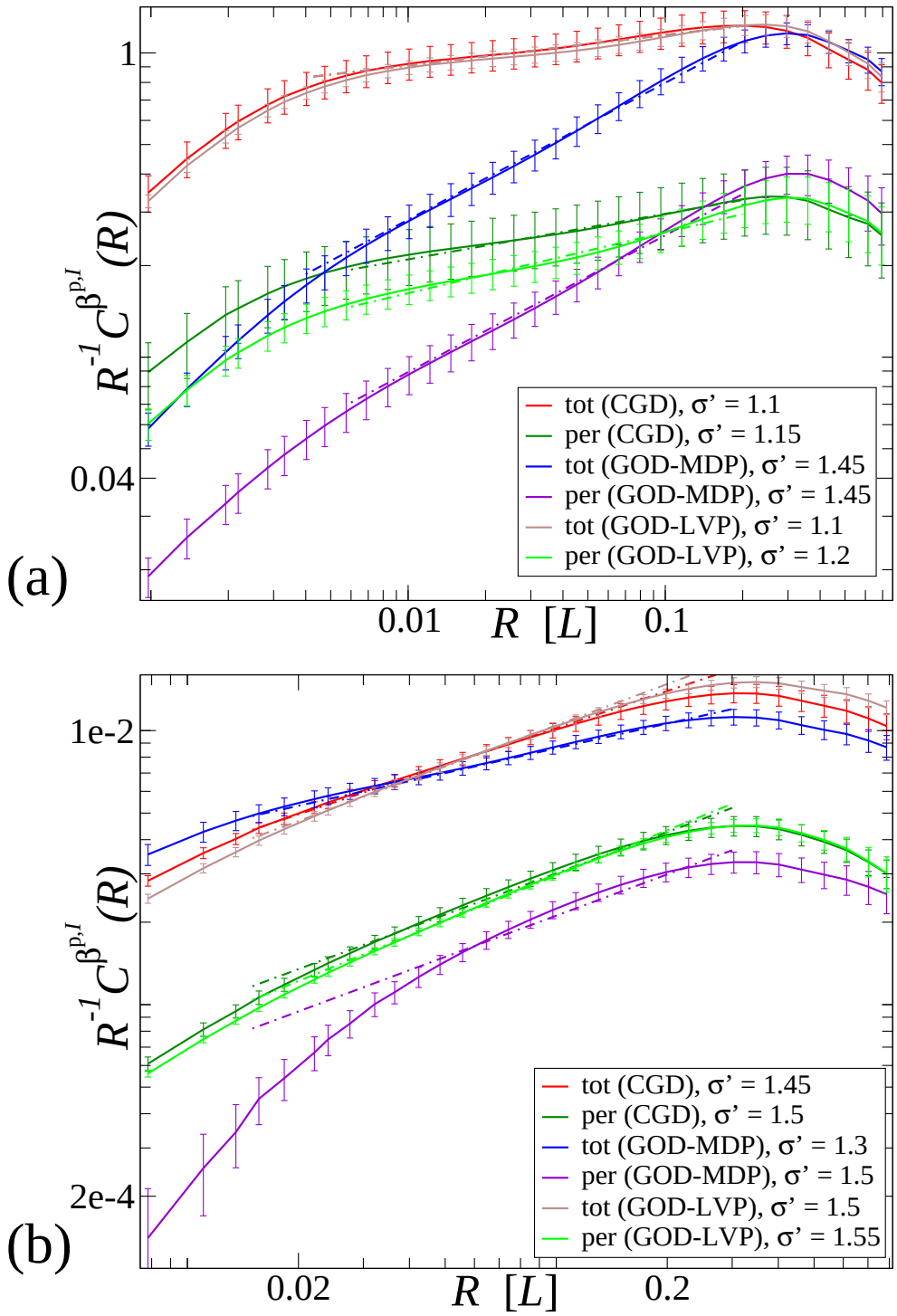

Figure 5.4: **Correlation functions of $\beta^{p,I}$ in both two and three dimensions**. The correlation functions of the intrinsic part of plastic distortion field are shown. *Top:* (a) is measured in relaxed, unstrained 1024^2 systems; *Bottom:* (b) is measured in in relaxed, unstrained 128^3 systems. All dashed lines show estimated power laws quoted in Table 6.1. Notice that we omit the correlation functions of $C_{tr}^{\beta^{p,I}}$, which are independent of distance, and unrelated to the emergent self-similarity, as shown in Sec. 6.2.

$\beta^{\mathrm{p,I}}$ thus includes the three scalar forms

$$
\begin{aligned}
C^{\beta^{\mathrm{p,I}}}_{tot}(\mathbf{x}) &= \langle(\beta^{\mathrm{p,I}}_{ij}(\mathbf{x}) - \beta^{\mathrm{p,I}}_{ij}(0))(\beta^{\mathrm{p,I}}_{ij}(\mathbf{x}) - \beta^{\mathrm{p,I}}_{ij}(0))\rangle \\
&= 2\langle\beta^{\mathrm{p,I}}_{ij}\beta^{\mathrm{p,I}}_{ij}\rangle - 2\langle\beta^{\mathrm{p,I}}_{ij}(\mathbf{x})\beta^{\mathrm{p,I}}_{ij}(0)\rangle; \qquad (5.7) \\
C^{\beta^{\mathrm{p,I}}}_{per}(\mathbf{x}) &= -\langle(\beta^{\mathrm{p,I}}_{ij}(\mathbf{x}) - \beta^{\mathrm{p,I}}_{ij}(0))(\beta^{\mathrm{p,I}}_{ji}(\mathbf{x}) - \beta^{\mathrm{p,I}}_{ji}(0))\rangle \\
&= -2\langle\beta^{\mathrm{p,I}}_{ij}\beta^{\mathrm{p,I}}_{ji}\rangle + 2\langle\beta^{\mathrm{p,I}}_{ij}(\mathbf{x})\beta^{\mathrm{p,I}}_{ji}(0)\rangle; \qquad (5.8) \\
C^{\beta^{\mathrm{p,I}}}_{tr}(\mathbf{x}) &= \langle(\beta^{\mathrm{p,I}}_{ii}(\mathbf{x}) - \beta^{\mathrm{p,I}}_{ii}(0))(\beta^{\mathrm{p,I}}_{jj}(\mathbf{x}) - \beta^{\mathrm{p,I}}_{jj}(0))\rangle \\
&= 2\langle\beta^{\mathrm{p,I}}_{ii}\beta^{\mathrm{p,I}}_{jj}\rangle - 2\langle\beta^{\mathrm{p,I}}_{ii}(\mathbf{x})\beta^{\mathrm{p,I}}_{jj}(0)\rangle; \qquad (5.9)
\end{aligned}
$$

where an overall minus sign is added to $C^{\beta^{\mathrm{p,I}}}_{per}$ so as to yield a positive measure.

In Fig. 5.4, the correlation functions of the intrinsic plastic distortion $\beta^{\mathrm{p,I}}$ in both 1024^2 and 128^3 simulations exhibit a critical exponent σ'. These measured critical exponents are shown in Table 6.1.

5.3 Correlation functions of the strain-history-dependent plastic deformation and distortion fields

The curl-free strain-history-dependent part of the plastic distortion field, as shown in Fig. 5.5(a), (c), and (e), exhibits structures reminiscent of self-similar morphology. We correlate their differences at neighboring points

$$
\begin{aligned}
C^{\beta^{\mathrm{p,H}}}_{tot}(\mathbf{x}) &= \langle(\beta^{\mathrm{p,H}}_{ij}(\mathbf{x}) - \beta^{\mathrm{p,H}}_{ij}(0))(\beta^{\mathrm{p,H}}_{ij}(\mathbf{x}) - \beta^{\mathrm{p,H}}_{ij}(0))\rangle, \qquad (5.10) \\
C^{\beta^{\mathrm{p,H}}}_{per}(\mathbf{x}) &= \langle(\beta^{\mathrm{p,H}}_{ij}(\mathbf{x}) - \beta^{\mathrm{p,H}}_{ij}(0))(\beta^{\mathrm{p,H}}_{ji}(\mathbf{x}) - \beta^{\mathrm{p,H}}_{ji}(0))\rangle, \qquad (5.11) \\
C^{\beta^{\mathrm{p,H}}}_{tr}(\mathbf{x}) &= \langle(\beta^{\mathrm{p,H}}_{ii}(\mathbf{x}) - \beta^{\mathrm{p,H}}_{ii}(0))(\beta^{\mathrm{p,H}}_{jj}(\mathbf{x}) - \beta^{\mathrm{p,H}}_{jj}(0))\rangle. \qquad (5.12)
\end{aligned}
$$

Consider also the deformation field $\boldsymbol{\psi}$ (shown in Fig. 5.5(b), (d), and (f)) of Eq. (2.19) whose gradient gives the strain-history-dependent plastic deformation $\beta^{\mathrm{p,H}}$.

Figure 5.5: Strain-history-dependent elds $^{p;H}$ and in two dimensions for the relaxed states. Top: Dislocation climb is allowed. Middle: Glide-only with mobile dislocation population. Bottom: Glide-only due to local vacancy pressure. Left: The strain-history-dependent plastic distortion $^{p;H}$. (a), (c), and (e) exhibit patterns reminiscent of self-similar dislocation structures. Right: The strain-history-dependent plastic deformation . (b), (d), and (f) exhibit smooth patterns with a little distortion, which are not fractal.

1-1 correspondence between cells and peaks.

CHAPTER 8

CONCLUSION

In this thesis, we have proposed a flexible framework of CDD to study complex mesoscale phenomena of collective dislocation motion. Traditionally, deterministic CDDs have been missing the experimentally ubiquitous feature of cellular pattern formation. Our CDD models have been developed in order to make progress in that respect.

In our earlier works [6, 7, 45], we focused our efforts on describing coarse-grained dislocations that naturally develop dislocation cellular structures in ways that are consistent with experimental observations. Our resulting simulation patterns reproduced both the fractal morphologies and some features of the scaling of cell sizes and misorientations analyzed experimentally, as a major target achieved in Ref. [7].

In our recent work [72], we go further in many aspects of the theory extending the results of our previous work:

We provide a derivation of our theory that explains the differences with traditional theories of plasticity. In addition to our previously studied climb-glide (CGD) and glide-only (GOD-MDP) models, we extend our construction in order to incorporate vacancies, and re-derive [8] a different glide-only dynamics (GOD-LVP) which we show exhibits very similar behavior in 2D to our CGD model. It is worth mentioning that in this way, the GOD-LVP and the CGD dynamics become statistically similar in 2D, while the previously studied, less physical, GOD-MDP model is different in 2D [7].

We present 3D simulation results here for the first time, showing qualitatively different behavior from that of 2D. In 3D, all three types of dynamics – CGD, GOD-MDP and GOD-LVP – show similar non-trivial fractal patterns and scaling dimensions. Thus our 3D analysis shows that the flatter 'grain boundaries' we observe in the 2D simula-

tions are not intrinsic to our dynamics, but are an artifact of the artificial z-independent initial conditions. Experimentally, grain boundaries are indeed flatter and cleaner than cell walls, and our theory no longer provides a new explanation for this distinction. We expect that the dislocation core energies left out of our model would flatten the walls, and that adding disorder or entanglement would prevent the low-temperature glide-only dynamics from flattening as much.

We also fully describe, in a statistical sense, multiple correlation functions – the local orientation, the plastic distortion, the GND density – their symmetries and their mutual scaling relations. Correlation functions of important physical quantities are categorized and analytically shown to share one stress-free exponent. The anomaly in the correlation functions of β^{p}, which was left as a question in our previous publication [7], has been discussed and explained. All of these correlation functions and properties are verified with the numerical results of the dynamics that we extensively discussed.

There still remain many fascinating mesoscale experiments, such as dislocation avalanches [52, 73], size-dependent hardness (smaller is stronger) [53], and complex anisotropic loading [74, 75], that we hope to emulate. We intend in the future to include several relevant additional ingredients to our dynamics, such as vacancies (Sec. 2.6), immobile dislocations/SSDs and slip systems (Sec. 2.7), impurities (Sec. 2.8), to reflect real materials.

APPENDIX A

PHYSICAL QUANTITIES IN TERMS OF THE PLASTIC DISTORTION TENSOR

In an isotropic infinitely large medium, the local deformation $\boldsymbol{u}$, the elastic distortion β^{e} and the internal long-range stress σ^{int} can be expressed [6, 76] in terms of the plastic distortion field β^{p} in Fourier space:

$$\begin{aligned}
\widetilde{\boldsymbol{u}}_i(\mathbf{k}) &= N_{ikl}(\mathbf{k})\widetilde{\beta}^{\mathrm{p}}_{kl}(\mathbf{k}), \\
N_{ikl}(\mathbf{k}) &= -\frac{i}{k^2}(k_k\delta_{il} + k_l\delta_{ik}) - i\frac{\nu k_i\delta_{kl}}{(1-\nu)k^2} + i\frac{k_ik_kk_l}{(1-\nu)k^4}; \qquad \text{(A.1)} \\
\widetilde{\beta}^{\mathrm{e}}_{ij}(\mathbf{k}) &= T_{ijkl}(\mathbf{k})\widetilde{\beta}^{\mathrm{p}}_{kl}(\mathbf{k}), \\
T_{ijkl}(\mathbf{k}) &= \frac{1}{k^2}(k_ik_k\delta_{jl} + k_ik_l\delta_{jk} - k^2\delta_{ik}\delta_{jl}) + \frac{k_ik_j}{(1-\nu)k^4}(\nu k^2\delta_{kl} - k_kk_l); \qquad \text{(A.2)} \\
\widetilde{\sigma}^{\mathrm{int}}_{ij}(\mathbf{k}) &= M_{ijmn}(\mathbf{k})\widetilde{\beta}^{\mathrm{p}}_{mn}(\mathbf{k}), \\
M_{ijmn}(\mathbf{k}) &= \frac{2u\nu}{1-\nu}\Big(\frac{k_mk_n\delta_{ij} + k_ik_j\delta_{mn}}{k^2} - \delta_{ij}\delta_{mn}\Big) + u\Big(\frac{k_ik_m}{k^2}\delta_{jn} + \frac{k_jk_n}{k^2}\delta_{im} - \delta_{im}\delta_{jn}\Big) \\
&\quad + u\Big(\frac{k_ik_n}{k^2}\delta_{jm} + \frac{k_jk_m}{k^2}\delta_{in} - \delta_{in}\delta_{jm}\Big) - \frac{2u}{1-\nu}\frac{k_ik_jk_mk_n}{k^4}. \qquad \text{(A.3)}
\end{aligned}$$

All these expressions are valid for systems with periodic boundary conditions.

According to the definition Eq. (2.12) of the crystalline orientation $\boldsymbol{\Lambda}$, we can replace ω^{e} with β^{e} and ϵ^{e} by using the elastic distortion tensor decomposition Eq. (2.10)

$$\Lambda_i = \frac{1}{2}\varepsilon_{ijk}(\beta^{\mathrm{e}}_{jk} - \epsilon^{\mathrm{e}}_{jk}). \qquad \text{(A.4)}$$

Here the permutation factor acting on the symmetric elastic strain tensor gives zero. Hence we can express the crystalline orientation vector $\boldsymbol{\Lambda}$ in terms of β^{p} by using Eq. (A.2)

$$\begin{aligned}
\widetilde{\Lambda}_i(\mathbf{k}) &= \frac{1}{2}\varepsilon_{ijk}\Big\{\frac{1}{k^2}(k_jk_s\delta_{kt} + k_jk_t\delta_{ks} - k^2\delta_{js}\delta_{kt}) + \frac{k_jk_k}{(1-\nu)k^4}(\nu k^2\delta_{st} - k_sk_t)\Big\}\widetilde{\beta}^{\mathrm{p}}_{st}(\mathbf{k}) \\
&= \frac{1}{2k^2}(\varepsilon_{ijt}k_jk_s + \varepsilon_{ijs}k_jk_t - k^2\varepsilon_{ist})\widetilde{\beta}^{\mathrm{p}}_{st}(\mathbf{k}). \qquad \text{(A.5)}
\end{aligned}$$

APPENDIX B

CALCULATION OF ENERGY FUNCTIONAL DERIVATIVE WITH RESPECT TO THE GND DENSITY

According to Eq. (2.17), the infinitesimal change of the variable $\delta\varrho$ is given in terms of $\delta\beta^{\mathrm{p}}$

$$\delta\varrho_{ijk} = -g_{ijls}\partial_l(\delta\beta^{\mathrm{p}}_{sk}). \tag{B.1}$$

Substituting Eq. (B.1) into Eq. (2.32) and applying integration by parts, the infinitesimal change of $\mathcal{F}$ is hence rewritten in terms of β^{p}

$$\delta\mathcal{F}[\beta^{\mathrm{p}}] = \int d^3\mathbf{x}\ g_{ijls}\partial_l\left(\frac{\delta\mathcal{F}}{\delta\varrho_{ijk}}\right)\delta\beta^{\mathrm{p}}_{sk}. \tag{B.2}$$

According to Eq. (2.29), it suggests

$$\delta\mathcal{F}[\beta^{\mathrm{p}}] = \int d^3\mathbf{x}\ \frac{\delta\mathcal{F}}{\delta\beta^{\mathrm{p}}_{sk}}\delta\beta^{\mathrm{p}}_{sk} = \int d^3\mathbf{x}\ (-\sigma_{sk})\delta\beta^{\mathrm{p}}_{sk}. \tag{B.3}$$

Comparing Eq. (B.2) and Eq. (B.3) implies

$$g_{ijls}\partial_l\left(\frac{\delta\mathcal{F}}{\delta\varrho_{ijk}}\right) = -\sigma_{sk}, \tag{B.4}$$

up to a total derivative which we ignore due to the use of periodic boundary conditions.

APPENDIX C

ENERGY DISSIPATION RATE

We can apply variational methods to calculate the dissipation rate of the free energy. As is well known, the general elastic energy $\mathcal{E}$ in a crystal can be expressed as $\mathcal{E} = \frac{1}{2}\int d^3\mathbf{x}\ \sigma_{ij}\epsilon^{\mathrm{e}}_{ij}$, with $\epsilon^{\mathrm{e}}_{ij}$ the elastic strain. An infinitesimal change of $\mathcal{E}$ is:

$$\delta\mathcal{E} = \frac{1}{2}\int d^3\mathbf{x}\ \sigma_{ij}\delta\epsilon^{\mathrm{e}}_{ij} + \frac{1}{2}\int d^3\mathbf{x}\ \delta\sigma_{ij}\epsilon^{\mathrm{e}}_{ij} = \int d^3\mathbf{x}\ \sigma_{ij}\delta\epsilon^{\mathrm{e}}_{ij}, \tag{C.1}$$

where we use $\sigma_{ij}\delta\epsilon^{\mathrm{e}}_{ij} = C_{ijkl}\epsilon^{\mathrm{e}}_{kl}\delta\epsilon^{\mathrm{e}}_{ij} = \delta\sigma_{ij}\epsilon^{\mathrm{e}}_{ij}$.

So the infinitesimal change of the free energy Eq. (2.25) is

$$\delta\mathcal{F} = \int d^3\mathbf{x}\left(\sigma^{\mathrm{int}}_{ij}\delta\epsilon^{\mathrm{e}}_{ij} - \sigma^{\mathrm{ext}}_{ij}\delta\epsilon^{\mathrm{p}}_{ij}\right). \tag{C.2}$$

We apply the relation $\epsilon^{\mathrm{e}} = \epsilon - \epsilon^{\mathrm{p}}$, where ϵ^{p} is the plastic strain and ϵ is the total strain:

$$\delta\mathcal{F} = \int d^3\mathbf{x}\left(\sigma^{\mathrm{int}}_{ij}\delta\epsilon_{ij} - \sigma^{\mathrm{int}}_{ij}\delta\epsilon^{\mathrm{p}}_{ij} - \sigma^{\mathrm{ext}}_{ij}\delta\epsilon^{\mathrm{p}}\right). \tag{C.3}$$

Using the symmetry of σ and ignoring large rotations, $\epsilon_{ij} = \frac{1}{2}(\partial_i u_j + \partial_j u_i)$, we can rewrite the first term of Eq. (C.3) as $\int d^3\mathbf{x}\ \sigma^{\mathrm{int}}_{ij}\delta(\partial_i u_j)$. Integrating by parts yields $\int d^3\mathbf{x}\ (\partial_i(\delta u_j\sigma^{\mathrm{int}}_{ij}) - \delta u_j\partial_i\sigma^{\mathrm{int}}_{ij}))$. We can convert the first volume integral to a surface integral, which vanishes for an infinitely large system. Hence

$$\delta\mathcal{F} = \int d^3\mathbf{x}\left(\partial_i\sigma^{\mathrm{int}}_{ij}\delta u_j - (\sigma^{\mathrm{int}}_{ij} + \sigma^{\mathrm{ext}}_{ij})\delta\epsilon^{\mathrm{p}}_{ij}\right). \tag{C.4}$$

The first term of Eq. (C.4) is zero assuming instantaneous elastic relaxation due to the local force equilibrium condition,

$$\delta\mathcal{F} = -\int d^3\mathbf{x}\ (\sigma^{\mathrm{int}}_{ij} + \sigma^{\mathrm{ext}}_{ij})\delta\beta^{\mathrm{p}}_{ij}, \tag{C.5}$$

using the symmetry of σ and $\epsilon^{\mathrm{p}}_{ij} = \frac{1}{2}(\beta^{\mathrm{p}}_{ij} + \beta^{\mathrm{p}}_{ji})$.

The free energy dissipation rate is thus $\delta\mathcal{F}/\delta t$ for $\delta\beta^{\mathrm{p}}_{ij} = \frac{\partial\beta^{\mathrm{p}}}{\partial t}\delta t$, hence

$$\begin{aligned}\frac{\partial\mathcal{F}}{\partial t} &= -\int d^3\mathbf{x}\ (\sigma^{\mathrm{int}}_{ij} + \sigma^{\mathrm{ext}}_{ij})\frac{\partial\beta^{\mathrm{p}}_{ij}}{\partial t} \\ &= -\int d^3\mathbf{x}\ (\sigma^{\mathrm{int}}_{ij} + \sigma^{\mathrm{ext}}_{ij})J_{ij}. \end{aligned} \tag{C.6}$$

When dislocations are allowed to climb, substituting the flux Eq. (2.41) into Eq. (C.6) implies that the free energy dissipation rate is strictly negative

$$\begin{aligned}\frac{\partial\mathcal{F}}{\partial t} &= -\int d^3\mathbf{x}\ (\sigma^{\mathrm{int}}_{ij} + \sigma^{\mathrm{ext}}_{ij})[v_l\varrho_{lij}] \\ &= -\int d^3\mathbf{x}\ \frac{|\varrho|}{D}v^2 \leq 0. \end{aligned} \tag{C.7}$$

When removing dislocation climb, we substitute Eq. (2.45) into Eq. (C.6) to guarantee that the rate of the change of the free energy density is also the negative of a perfect square

$$\begin{aligned}\frac{\partial\mathcal{F}}{\partial t} &= -\int d^3\mathbf{x}(\sigma^{\mathrm{int}}_{ij} + \sigma^{\mathrm{ext}}_{ij})\left[v'_l(\varrho_{lij} - \frac{1}{3}\delta_{ij}\varrho_{lkk})\right] \\ &= -\int d^3\mathbf{x}\ \frac{|\varrho|}{D}v'^2 \leq 0. \end{aligned} \tag{C.8}$$

APPENDIX D

SUMMARY OF DYNAMICAL EQUATIONS OF OUR CDD MODEL

The general form of the conservation law of the Burgers vector is expressed in terms of either the GND density

$$\frac{\partial}{\partial t}\varrho_{ijk} = -\varepsilon_{ijm}\varepsilon_{mpq}\partial_p J_{qk} = -g_{ijpq}\partial_p J_{qk}, \tag{D.1}$$

or the plastic distortion tensor β^{p}

$$\frac{\partial \beta^{\mathrm{p}}_{ij}}{\partial t} = J_{ij}, \tag{D.2}$$

where J represents the Burgers vector flux, and the symbol g_{ijpq} indicates $\varepsilon_{ijm}\varepsilon_{mpq} = \delta_{ip}\delta_{jq} - \delta_{iq}\delta_{jp}$. We numerically observe that simulations of Eqs. (D.1), (D.2) lead to the same results statistically (i.e., the numerical time step approximations leave the physics invariant).

In our CDD models, we implement three distinct dynamical equations:

(i) Climb and glide dynamics (CGD) – Eq. (2.41)

$$J_{ij} = v_u \varrho_{uij} = \frac{D}{|\varrho|}\sigma_{mk}\varrho_{umk}\varrho_{uij}; \tag{D.3}$$

(ii) Glide-only dynamics due to mobile dislocation population (GOD-MDP) – Eq. (2.45)

$$J'_{ij} = v'_u \varrho'_{uij} = \frac{D}{|\varrho|}\sigma_{mn}\left(\varrho_{umn} - \frac{1}{3}\delta_{mn}\varrho_{ull}\right)\left(\varrho_{uij} - \frac{1}{3}\delta_{ij}\varrho_{ukk}\right); \tag{D.4}$$

(iii) Glide-only dynamics due to local vacancy pressure (GOD-LVP) – Eq. (2.49)

$$J''_{ij} = \frac{D}{|\varrho|}\left(\sigma_{mn} - \frac{\sigma_{pq}\varrho_{spq}\varrho_{skk}}{\varrho_{uaa}\varrho_{ubb}}\delta_{mn}\right)\varrho_{umn}\varrho_{uij}. \tag{D.5}$$

Here, the GND density ϱ is the curl of the plastic distortion β^{p} (Eq. 2.17); σ indicates the internal stress (Eq. A.3) due to the mutual interaction between dislocations, plus the applied stress; D is a positive material-dependent constant.

BIBLIOGRAPHY

[1] L. D. Landau and E. M. Lifshitz, *Theory of Elasticity*, 2nd ed. (Pergamon Press, 1970).

[2] A. Acharya, "A model of crystal plasticity based on the theory of continuously distributed dislocations," *J. Mech. Phys. Solids* **49**, 761 (2001).

[3] A. Acharya, "Driving forces and boundary conditions in continuum dislocation mechanics," *Proc. R. Soc. A* **459**, 1343 (2003).

[4] A. Acharya, "Constitutive analysis of finite deformation field dislocation mechanics," *J. Mech. Phys. Solids* **52**, 301 (2004).

[5] A. Roy and A. Acharya, "Finite element approximation of field dislocation mechanics," *J. Mech. Phys. Solids* **53**, 143 (2005).

[6] S. Limkumnerd and J. P. Sethna, "Mesoscale theory of grains and cells: Crystal plasticity and coarsening," *Phys. Rev. Lett.* **96**, 095503 (2006).

[7] Y. S. Chen, W. Choi, S. Papanikolaou, and J. P. Sethna, "Bending crystals: Emergence of fractal dislocation structures," *Phys. Rev. Lett.* **105**, 105501 (2010).

[8] A. Acharya and A. Roy, "Size effects and idealized dislocation microstructure at small scales: predictions of a phenomenological model of mesoscopic field dislocation mechanics: Part i," *J. Mech. Phys. Solids* **54**, 1687 (2006).

[9] Y. Kawasaki and T. Takeuchi, "Cell structures in copper single-crystals deformed in the [001] and [111] axes," *Scr. Metall.* **14**, 183 (1980).

[10] H. Mughrabi, T. Ungar, W. Kienle, and M. Wilkens, "Long-range internal-stresses and asymmetric x-ray line-broadening in tensile-deformed [001]-orientated copper single-crystals," *Philos. Mag. A* **53**, 793 (1986).

[11] C. Schwink, "Flow-stress dependence on cell geometry in single-crystals," *Scr. Metall. Mater.* **27**, 963 (1992).

[12] T. Ungár, L. S. Tóth, J. Illy, and I. Kovács, "Dislocation structure and work hardening in polycrystalline ofhc copper rods deformed by torsion and tension," *Acta Metall.* **34**, 1257 (1986).

[13] J. Gil Sevillano, E. Bouchaud, and L. P. Kubin, "The fractal nature of gliding dislocation lines," *Scr. Metall. Mater.* **25**, 355 (1991).

[14] J. Gil Sevillano, "Patterns in heavily deformed metals," *Phys. Scr.* **T49B**, 405 (1993).

[15] P. Hähner, K. Bay, and M. Zaiser, "Fractal dislocation patterning during plastic deformation," *Phys. Rev. Lett.* **81**, 2470 (1998).

[16] M. Zaiser, K. Bay, and P. Hähner, "Fractal analysis of deformation-induced dislocation patterns," *Acta Mater.* **47**, 2463 (1999).

[17] B. Bakó and I. Groma, "Computer simulations of a three-dimensional ising ferromagnet with quenched disorder," *Phys. Rev. B* **60**, 9228 (1999).

[18] B. Bakó, I. Groma, G. Gyorgyi, and G. T. Zimanyi, "Dislocation glasses: Aging during relaxation and coarsening," *Phys. Rev. Lett.* **98**, 075701 (2007).

[19] B. Bakó and W. Hoffelner, "Cellular dislocation patterning during plastic deformation," *Phys. Rev. B* **76**, 214108 (2007).

[20] R. Madec, B. Devincre, and L. P. Kubin, "Simulation of dislocation patterns in multislip," *Scr. Mater.* **47**, 689 (2002).

[21] D. Gomez-Garcia, B. Devincre, and L. P. Kubin, "Dislocation patterns and the similitude principle: 2.5 D mesoscale simulations," *Phys. Rev. Lett.* **96**, 125503 (2006).

[22] D. Walgraef and E. Aifantis, "On the formation and stability of dislocation patterns–I: One-dimensional considerations," *Int. J. Eng. Sci.* **23**, 1351 (1985).

[23] P. Hähner, "On the foundations of stochastic dislocation dynamics," *Appl. Phys. A* **62**, 473 (1996).

[24] M. Saxlová, J. Kratochvil, and J. Zatloukal, "The model of formation and disintegration of vein dislocation structure," *Mater. Sci. Eng. A* **234**, 205 (1997).

[25] I. Groma and B. Bakó, "Dislocation patterning: From micro- to mesoscale description," *Phys. Rev. Lett.* **84**, 1487 (2000).

[26] W. Pantleon, "On the distribution function of disorientations in dislocation cell structures," *Scr. Metall.* **35**, 511 (1996).

[27] W. Pantleon, "On the statistical origin of disorientations in dislocation structures," *Acta Mater.* **46**, 451 (1998).

[28] J. P. Sethna, V. R. Coffman, and E. Demler, "Scaling in plasticity-induced cell-boundary microstructure: Fragmentation and rotational diffusion," *Phys. Rev. B* **67**, 184107 (2003).

[29] Kröner, "Continuum Theory of Defects," in *Physics of Defects, Les Houches, Session XXXV, 1980*, edited by R. Balian, M. Kleman, and J. P. Poirier (North-Holland: Amsterdam, 1981) pp. 215–315.

[30] S. Limkumnerd and J. P. Sethna, "Stress-free states of continuum dislocation fields:

Rotations, grain boundaries, and the nye dislocation density tensor," *Phys. Rev. B* **75**, 224121 (2007).

[31] J. M. Rickman and J. Viñals, "Modelling of dislocation structures in materials," *Philos. Mag. A* **75**, 1251 (1997).

[32] A. Roy and A. Acharya, "Size effects and idealized dislocation microstructure at small scales: predictions of a phenomenological model of mesoscopic field dislocation mechanics: Part ii," *J. Mech. Phys. Solids* **54**, 1711 (2006).

[33] S. Varadhan, A. Beaudoin, and C. Fressengeas, "Coupling the dynamics of statistically distributed and excess dislocations," in *Proceedings of Science, SMPRI2005* (2006) p. 004.

[34] D. Kuhlmann-Wilsdorf and N. Hansen, "Geometrically necessary, incidental and subgrain boundaries," *Scr. Metall. Mater.* **25**, 1557 (1991).

[35] D. A. Hughes and N. Hansen, "Microstructural evolution in nickel during rolling from intermediate to large strains," *Metall. Trans. A* **24**, 2022 (1993).

[36] J. P. Hirth and J. Lothe, *Theory of Dislocatons* (Wiley, New York, 1982).

[37] I. Mura, "On dynamic problems of continuous distribution of dislocations," *Int. J. Eng. Sci.* **1**, 371 (1963).

[38] Stefano Zapperi and Michael Zaiser (private communication).

[39] M. Koslowski, A. M. Cuitino, and M. Ortiz, "A phase-field theory of dislocation dynamics, strain hardening and hysteresis in ductile single crystals," *J. Mech. Phys. Solids* **50**, 2597 (2002).

[40] M. Koslowski and M. Ortiz, "A multi-phase field model of planar dislocation networks," *Modelling Simul. Mater. Sci. Eng.* **12**, 1087 (2004).

[41] A. Arsenlis and D. Parks, "Modeling the evolution of crystallographic dislocation density in crystal plasticity," *J. Mech. Phys. Solids* **50**, 1979 (2002).

[42] A. Arsenlis, D. Parks, R. Becker, and V. Bulatova, "On the evolution of crystallographic dislocation density in non-homogeneously deforming crystals," *J. Mech. Phys. Solid* **52**, 1213 (2004).

[43] S. Limkumnerd and J. P. Sethna, "Shocks and slip systems: Predictions from a mesoscale theory of continuum dislocation dynamics," *J. Mech. Phys. Solids* **56**, 1450 (2008).

[44] A. Kurganov, S. Noelle, and G. Petrova, "Semidiscrete central-upwind schemes for hyperbolic conservation laws and Hamilton-Jacobi equations," *SIAM J. Sci. Comput.* **23**, 707 (2001).

[45] W. Choi, Y. S. Chen, S. Papanikolaou, and J. P. Sethna, "Is dislocation flow turbulent in deformed crystals?" (2011), e-print arXiv:1105.5351.

[46] A. Pumir and E. D. Siggia, "Development of singular solutions to the axisymmetric Euler equations," *Phys. Fluids A* **4**, 1472 (1992).

[47] A. Pumir and E. D. Siggia, "Finite-time singularities in the axisymmetrical 3-dimension Euler equations," *Phys. Rev. Lett.* **68**, 1511 (1992).

[48] W. Choi, Y. S. Chen, S. Papanikolaou, and J. P. Sethna, "δ-shocks and generalized riemann solutions in multi-component nonlinear partial differenital equations," (2012), (manuscript in preparation).

[49] D. A. Hughes, D. C. Chrzan, Q. Liu, and N. Hansen, "Scaling of misorientation angle distributions," *Phys. Rev. Lett.* **81**, 4664 (1998).

[50] D. A. Hughes, Q. Liu, D. C. Chrzan, and N. Hansen, "Scaling of microstructural parameters: misorientations of deformation induced boundaries," *Acta Mater.* **45**, 105 (1997).

[51] D. A. Hughes and N. Hansen, "Graded nanostructures produced by sliding and exhibiting universal behavior," *Phys. Rev. Lett.* **87**, 135503 (2001).

[52] M. C. Miguel, A. Vespignani, S. Zapperi, J. Weiss, and J. R. Grasso, "Intermittent dislocation flow in viscoplastic deformation," *Nature* **410**, 71 (2001).

[53] M. D. Uchic, D. M. Dimiduk, J. N. Florando, and W. D. Nix, "Sample dimensions influence strength and crystal plasticity," *Science* **305**, 986 (2004).

[54] J. Mach, A. J. Beaudoin, and A. Acharya, "Continuity in the plastic strain rate and its influence on texture evolution," *J. Mech. Phys. Solids* **58**, 105 (2010).

[55] D. P. Mika and P. R. Dawson, "Polycrystal plasticity modeling of intracrystalline boundary textures," *Acta Mater.* **47**, 1355 (1999).

[56] P. Chaikin and T. Lubensky, *Principles of Condensed Matter Physics* (Cambridge University Press, Cambridge, England, 1995).

[57] C. Song, S. Havlin, and H. A. Makse, "Self-similarity of complex networks," *Nature* **433**, 392 (2005).

[58] M. Vergassola, B. Dubrulle, U. Frisch, and A. Noullez, "Burgers' equation, devil's staircases and the mass distribution for large-scale structures," *Astron. Astrophys.* **289**, 325 (1994).

[59] P. J. E. Peebles, *Principles of Physical Cosmology* (Princeton University Press, Princeton, 1993).

[60] P. Coles and F. Lucchin, *Cosmology: the Origin and Evolution of Cosmic Structures* (Wiley, Chichester, 1995).

[61] B. Jakobsen, H. F. Poulsen, U. Lienert, J. Almer, S. D. Shastri, H. O. Sorensen, C. Gundlach, and W. Pantleon, "Formation and subdivision of deformation structures during plastic deformation," *Science* **312**, 889 (2006).

[62] L. Margulies, G. Winther, and H. F. Poulsen, "In situ measurement of grain rotation during deformation of polycrystals," *Science* **291**, 2392 (2001).

[63] J. A. Wert, X. Huang, G. Winther, W. Pantleon, and H. F. Poulsen, "Revealing deformation microstructures," *Materials Today* **10**, 24 (2007).

[64] B. Larson, W. Yang, G. Ice, J. Budai, and J. Tischler, "Three-dimensional x-ray structural microscopy with submicrometre resolution," *Nature* **415**, 887 (2002).

[65] L. Levine, B. Larson, W. Yang, M. Kassner, J. Tischler, M. Delos-Reyes, R. Fields, W. Liu, *et al.*, "X-ray microbeam measurements of individual dislocation cell elastic strains in deformed single-crystal copper," *Nature Mater.* **5**, 619 (2006).

[66] W. Yang, B. Larson, J. Tischler, G. Ice, J. Budai, and W. Liu, "Differential-aperture x-ray structural microscopy: a submicron-resolution three-dimensional probe of local microstructure and strain," *Micron* **35**, 431 (2004).

[67] H. Poulsen, *Three-dimensional X-ray diffraction microscopy: Mapping polycrystals and their dynamics*, 205 (Springer Verlag, 2004).

[68] M. Pfeifer, G. Williams, I. Vartanyants, R. Harder, and I. Robinson, "Three-dimensional mapping of a deformation field inside a nanocrystal," *Nature* **442**, 63 (2006).

[69] I. Robinson and R. Harder, "Coherent x-ray diffraction imaging of strain at the nanoscale," *Nature Mater.* **8**, 291 (2009).

[70] I. Groma, "X-ray line broadening due to an inhomogeneous dislocation distribution," *Phys. Rev. B* **57**, 7535 (1998).

[71] F. Székely, I. Groma, and J. Lendvai, "Characterization of self-similar dislocation patterns by x-ray diffraction," *Phys. Rev. B* **62**, 3093 (2000).

[72] Y. S. Chen, W. Choi, S. Papanikolaou, M. Bierbaum, and J. P. Sethna, "Scaling theory of continuum dislocation dynamics in three dimensions: Self-organized fractal pattern formation," (2011), e-print arXiv:1106.0195.

[73] D. M. Dimiduk, C. Woodward, R. LeSar, and M. D. Uchic, "Scale-free intermittent flow in crystal plasticity," *Science* **312**, 1188 (2006).

[74] J. H. Schmitt, J. V. Fernandes, J. J. Gracio, and M. F. Vieira, "Plastic behaviour of copper sheets during sequential tension tests," *Mater. Sci. Eng. A* **147**, 143 (1991).

[75] A. B. Lopes, F. Barlat, J. J. Gracio, J. F. Ferreira Duarte, and E. F. Rauch, "Effect of texture and microstructure on strain hardening anisotropy for aluminum deformed in uniaxial tension and simple shear," *Int. J. Plasticity* **19**, 1 (2003).

[76] T. Mura, *Micromechanics of Defects in Solids*, 2nd ed. (Kluwer Academic Publishers, Dordrecht, 1991).